arXiv:2407.17493v2 [cs.CV] 24 Oct 2024

MODEL COLLAPSE IN THE SELF-CONSUMING CHAIN OF DIFFUSION FINETUNING: A NOVEL PERSPECTIVE FROM QUANTITATIVE TRAIT MODELING

Youngseok Yoon
UCSB
California, USA
youngseok_yoon@ucsb.edu

Dainong Hu
UCSB
California, USA
dainong@ucsb.edu

Iain Weissburg
UCSB
California, USA
ixw@ucsb.edu

Yao Qin
UCSB, Google
California, USA
yaoqin@ucsb.edu

Haewon Jeong
UCSB
California, USA
haewon@ucsb.edu

ABSTRACT

The success of generative models has reached a unique threshold where their outputs are indistinguishable from real data, leading to the inevitable contamination of future data collection pipelines with synthetic data. While their potential to generate infinite samples initially offers promise for reducing data collection costs and addressing challenges in data-scarce fields, the severe degradation in performance has been observed when iterative loops of training and generation occur—known as "model collapse." This paper explores a practical scenario in which a pretrained text-to-image diffusion model is finetuned using synthetic images generated from a previous iteration, a process we refer to as the "Chain of Diffusion." We first demonstrate the significant degradation in image quality caused by this iterative process and identify the key factor driving this decline through rigorous empirical investigations. Drawing an analogy between the Chain of Diffusion and biological evolution, we then introduce a novel theoretical analysis based on quantitative trait modeling. Our theoretical analysis aligns with empirical observations of the generated images in the Chain of Diffusion. Finally, we propose Reusable Diffusion Finetuning (ReDiFine), a simple yet effective strategy inspired by genetic mutations. ReDiFine mitigates model collapse without requiring any hyperparameter tuning, making it a plug-and-play solution for reusable image generation.

1 Introduction

Can state-of-the-art AI models learn from their own outputs and improve themselves? As generative AI models (e.g., GPT, Diffusion) now churn out uncountable synthetic texts and images, this question piqued the curiosity of many researchers in the past couple of years. While some show positive results of self-improving [1, 2], most report an undesirable *"model collapse"*—a phenomenon where a model's performance degrades when it undergoes multiple cycles of training with the self-generated data [3–10]. When large language models (LLMs) are trained with their own outputs, it begins to produce low-quality text with many repetitions [11], and its linguistic diversity declines rapidly [12, 13]; image models also show quality degradation [14, 15] and loss of diversity [16, 17].

The goal of this paper is to investigate model collapse in the practical scenario of finetuning pretrained text-to-image diffusion models. An end user of text-to-image diffusion models often wants to finetune the latest model to generate images with a very specific style (e.g., creating new characters in the style of Pokémon). In fact, hundreds of new finetuned diffusion models are regularly uploaded on platforms like CivitAI[1], each designed to produce different styles

[1] https://civitai.com/

of images. When users scrape the internet to collect images in the style they want, it becomes almost inevitable that synthetic images will be included in their datasets. This is because the number of real images is limited, while synthetic images can be generated in massive quantities and dominate online sources. As a result, users will feel compelled to include more synthetic images in their datasets to meet the data demands of these ever-growing, data-hungry models.

To this end, we conduct a thorough investigation into how various hyperparameters commonly used during diffusion finetuning (e.g., learning rate, diffusion steps, prompts) impact model collapse. From our extensive empirical analysis, we make a crucial observation: the classifier-free guidance (CFG) scale is the most significant factor influencing the rate of model collapse. Moreover, we observe a fascinating phenomenon that the direction of degradation varies with different CFG values—low CFG results in low-frequency degradation in images, while high CFG leads to high-frequency degradation. The critical role of CFG in determining both the rate and direction of model collapse is a novel insight previously unrecognized in the literature.

To gain a deeper theoretical understanding of this phenomenon, we draw upon the concept of quantitative trait modeling from statistical genetics. Unlike existing studies that attribute model collapse to limited sample sizes and conclude that it leads to zero variance [3, 6, 16], we propose that the underlying cause is a truncation-based selection process modulated by CFG. This theoretical model accurately describes our experimental observations. Moreover, we show that other theoretical work on model collapse can also be connected to statistical genetics models, such as random genetic drift and its variants [18–21]. This fresh angle of drawing parallels with statistical genetics offers a new framework to understand the mechanism of model collapse.

Finally, inspired by our empirical results and theoretical insights, we introduce the Reusable Diffusion Finetuning (ReDiFine) method. Our experiments show that selecting an appropriate CFG can significantly slow down model collapse. However, finding the optimal CFG is computationally expensive, requiring numerous iterations of finetuning. To address this, we propose ReDiFine as a plug-and-play solution that achieves a comparable reduction in collapse rate without the need for any hyperparameter tuning. The default ReDiFine setting effectively mitigates model collapse across all four datasets we tested. Moreover, ReDiFine is effective at mitigating model collapse not only in a worst-case scenario of having a fully synthetic dataset, but also in a more practical case, where we have a mix of real and synthetic images in the training set. Our contributions can be summarized as follows:

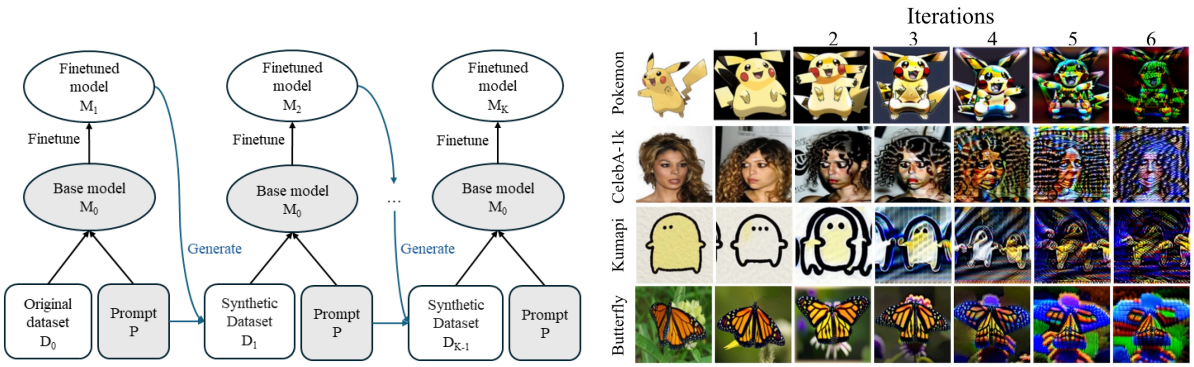
- We performed thorough and extensive empirical investigations into model collapse when we finetune a diffusion model with diffusion-generated images. We tested an exhaustive list of experimental parameters on four datasets (two digital art & two natural images) to identify what affects model collapse. Our analysis reveals that CFG scale is the most influential factor that not only controls the rate of model collapse but also dictates the type of image degradation (Section 3).
- We provide a novel theoretical analysis of model collapse based on quantitative trait modeling that can accurately predict how power spectra of generated images evolve over iterations (Section 4).
- We propose a simple yet effective strategy to mitigate model collapse, named ReDiFine, which combines condition drop finetuning and CFG scheduling. Across all four datasets, ReDiFine successfully generates more "reusable" images, which can be reused to finetune a diffusion model without causing a severe model collapse (Section 5).

2 Related Work

The self-consuming training loop and the associated phenomenon known as "model collapse" have become significant areas of study in the past two years [3–5, 7–10, 12–16]. Model collapse, defined as "a degenerative process affecting generations of learned generative models, where generated data end up polluting the training set of the next generation of models" in [6], has been observed in both language and image generative models.

Empirical studies on LLMs [13] reveal that linguistic diversity collapses, especially in high-entropy tasks [12], although this can be mitigated with data accumulation [2]. In image generation, several works [3, 10, 14–17] note image degradation when diffusion models are recursively trained with self-generated data. We conduct extensive empirical experiments to identify the most significant factor causing model collapse in text-to-image diffusion models. Our findings reveal that while model collapse is universally observed across various datasets and scenarios, it manifests in three distinct types of image degradation.

Theoretical studies on model collapse have largely focused on the reduction of diversity, typically framed as either decreasing covariance in continuous domains [3,6,16] or shrinking support in discrete domains [9,11]. The finite number of generated samples per iteration has been identified as a key cause of model collapse by several authors [3, 6, 8, 11, 22], while others [9, 16, 23] emphasize that sampling bias reduces the generative model's effective distribution. In contrast, we present a novel theoretical framework based on quantitative trait modeling, shifting the focus from variance reduction



(a) Self-Consuming Chain of Diffusion Finetuning.

(b) Image degradation in the Chain of Diffusion.

Figure 1: (a) **Overall pipeline of the Chain of Diffusion.** Given a pretrained text-to-image diffusion model M_0 and a prompt set P, a finetuned model M_k is trained using D_{k-1} generated at the previous iteration $k-1$. Then, M_k generates D_k using the same prompt set P, building a fully synthetic loop. Chain of diffusion begins with the original real dataset D_0. (b) **Image degradation universally occurs during Chain of Diffusion across four datasets.** As the Chain of Diffusion progresses, the severity of image degradation intensifies, exhibiting universal patterns of highly saturated images containing repetitive high-frequency patterns. This consistently holds across four datasets and 10 scenarios that we comprehensively investigate in Section 3.2.

to mean drift induced by the selection process. We further demonstrate that many existing theories of model collapse can be understood as extensions of classical results from statistical genetics.

Regarding mitigation strategies for model collapse, existing works echo the importance of incorporating a large proportion of real data throughout the training loop [3,8,16,23] or accumulating additional data [2]. The only mitigation strategy beyond altering the training data composition is proposed by [4], who suggests a self-correcting self-consuming loop using an expert model to correct synthetic outputs. While this approach is demonstrated in human motion generation with a physics simulator, having an expert model may not be feasible and could be too costly for many real-world applications. In our work, we propose an alternative solution through *reusable image generation*, and show that it can mitigate model collapse more effectively than mixing more real data.

3 Model Collapse in Self-Consuming Chain of Diffusion

3.1 Problem Setting & Experimental Setup

Chain of Diffusion. We begin with formally defining the self-consuming Chain of Diffusion finetuning. Given a pretrained generative model M_0, an original training image set $D_0 = \{x_{0,i} | i \in [0, N-1]\}$, and a prompt set $P = \{y_i | i \in [0, N-1]\}$, where N is the number of total images in the dataset, each image $x_{0,i}$ is paired with a corresponding text prompt y_i. M_{k+1} is a model finetuned from M_0 using the generated image set $D_k = \{x_{k,i} | i \in [0, N-1]\}$ and the prompt set P, which simulates a fully synthetic loop [16] for finetuning a pretrained generative model. Then, M_{k+1} generates a set of images D_{k+1} for the next iteration using the prompt set P:

$$M_{k+1} = \text{Finetune}(M_0, D_k, P), \tag{1}$$

$$D_{k+1} = \text{Generate}(M_{k+1}, P). \tag{2}$$

During the Chain of Diffusion, M_0 and P are fixed across all the iterations. To maintain the same size of training dataset, we generate one image per text prompt for all iterations. The overall pipeline of the Chain of Diffusion is shown in Figure 1(a).

Model and datasets. We use Stable Diffusion v1.5 [24] as the pretrained model M_0 and apply LoRA [25] to finetune the Stable Diffusion at each iteration. We build our implementation on [26] and perform experiments on four datasets: Pokemon [27], Kumapi [28], Butterfly [29], and CelebA-1k [30] to investigate various domains including animation,

[2] C, W, S, and L for Combine, Waifu, Short, and Long, respectively. We concatenate BLIP and Waifu captions as default setting, referred to as Combine. Short and Long prompts are BLIP captions generated with limitations in the lengths of captions. More details can be found in Appendix C.4.

[3] We do not display scenarios that change the training dataset size, such as Img/Prompt and Dataset Size, as varying sizes result in FID scores on different scales. The related results are presented in the Appendix C, where we observe similar image degradation.

Candidates	Default	Values
Dataset size	$1k$	$0.5k$, $2k$
Learning rate	1e-4	1e-3, 1e-5
Finetune	Both	Unet, Text encoder
Noise to images	No	Yes
Prompt	C	W, S, L
CLIP skip	2	1, 3
Diffusion steps	30	100
Epochs	100	50, 200
Mixing real images	0.0	0.5, 0.9
Image per prompt	1	5

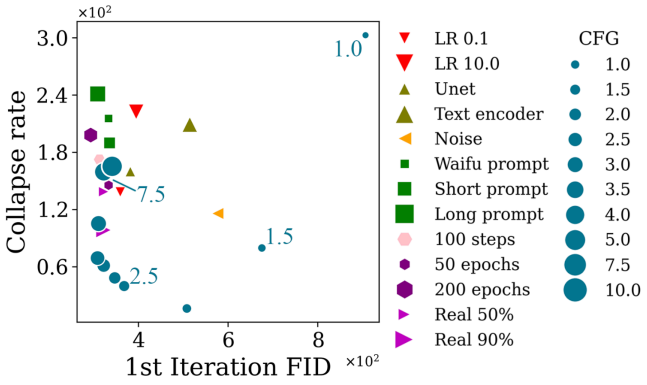


Figure 2: **Left:** Description of 10 potential factors (excluding CFG) that we examined as candidate sources for model collapse. All experiments were conducted on Pokemon except for the dataset size. For dataset size, we use CelebA since its original dataset is bigger, and we can subsample 500, 1000, and 2000 images. For prompt, we concatenate prompts with different lengths.[2] **Right:** All hyperparameter settings other than changing CFG show a high *collapse rate* greater than 100, i.e., FID score increases by ∼2x in 6 iterations, indicating severe image degradation. The x-axis represents FID_1, quantifying the generation performance at the first iteration and the y-axis represents the *collapse rate* defined in Equation (3). For both FID_1 and *collapse rate*, lower is better.[3]

handwriting, and real pictures. During each iteration, we finetune the pretrained Stable Diffusion M_0 for 100 epochs. More implementation details can be found in Appendix A.1 and A.2.

Evaluation metrics. We use Frechet Inception Distance (FID) [31] to measure image fidelity. Following [32], we use DiNOv2 [33] as a feature extractor for FID since it is more consistent with our visual inspection than Inception-V3 network [34]. With a slight abuse of terms, we will still refer to the Frechet distance with DiNOv2 features as the FID score. Quantitative results for additional metrics including CLIP score [35] can be found in Appendix E.

In addition to evaluation metrics for generative models presented above, we propose a new metric to quantify the reusability of images generated in the Chain of Diffusion. We define collapse rate as the performance degeneration per iteration in the Chain of Diffusion:

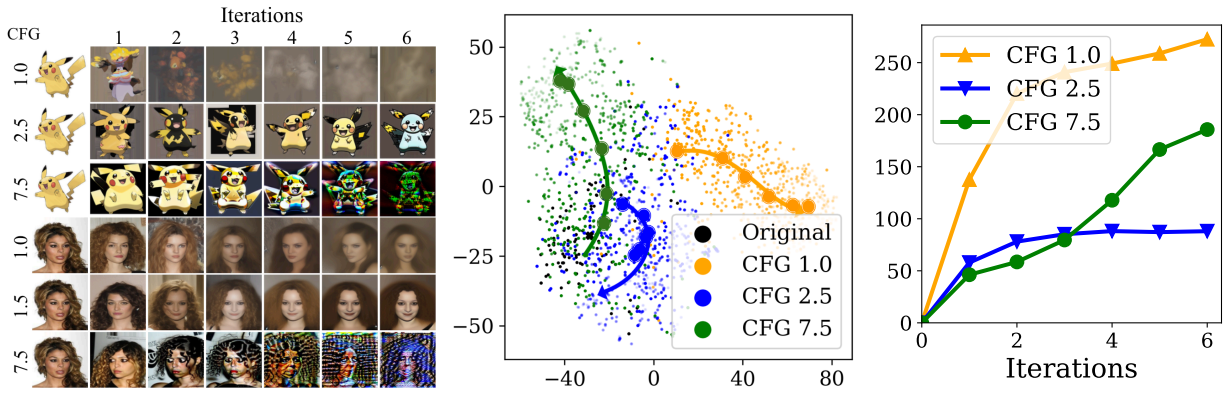
$$\text{collapse rate} = \Delta\text{FID} = \frac{\text{FID}_K - \text{FID}_1}{K-1}, \tag{3}$$

where FID_k stands for the FID between k-th iteration set and the original training set. We use FID as a performance metric here, but this can be CLIP, or any other performance metric of interest. Note that a low collapse rate indicates more reusable images since it means that the model does not degrade much during the Chain of Diffusion and we have $K = 6$ in the rest of the paper.

3.2 Model Collapse in the Chain of Diffusion

In this section, we make a series of observations regarding the model collapse behavior in the Chain of Diffusion. We conduct extensive investigations to reveal the most impactful factor in the model collapse and analyze how this factor contributes to the Chain of Diffusion.

Observation 1: Model collapse is universal in the Chain of Diffusion. We observe significant image degradation in all four datasets (see Figure 1(b)) in the Chain of Diffusion. The quality of generated images begins to clearly deteriorate in the third iteration and drops even more rapidly once the visible degradation emerges, reaching an unrecognizable level in two or three additional iterations. We investigated a variety of different scenarios (summarized in Figure 2) to see if this degradation is an anomaly of specific hyperparameter settings or if it is a ubiquitous phenomenon. We tested various dataset sizes for D_0 and D_k, increasing the size of synthetic datasets D_k by generating more than one image per prompt, mixing real images from D_0 to D_k, changing the descriptiveness of prompts, freezing U-Net or text encoder during finetuning, and various other hyperparameters (# sampling steps, # epochs, learning rate, and CLIP skip). We also tested adding a small Gaussian noise in each image in the original set D_0 to see if having small random perturbations can improve reusability, and investigated if the degradation happens for larger Stable Diffusion. *In all settings we tested, image degradation was universally present and very fast.* We plot the results for Pokemon on Figure 2 where y-axis is collapse rate and x-axis is the FID_1 (better when closer to the origin). While adding noise to images and mixing 90% real images to every iteration as proposed by [2, 3, 8, 16, 23] show the lowest collapse rate, they



(a) Degradations across different CFGs. (b) t-SNE of images. (c) FID ↓.

Figure 3: (a) **Low CFG leads to blurry images and high CFG leads to high-frequency degradation in the Chain of Diffusion.** CFG 2.5 for Pokemon and 1.5 for CelebA exhibit an ideal middle ground where both types of degradation slow down. More images in Appendix B. (b) t-SNE plot visualizes how generated images evolve from the original distribution (black) and shows distinct paths for three CFG scales (Pokemon). Different CFG scales and iterations are differentiated with different colors and transparency. Arrows indicate how the distributions of generated images move for different CFG scales. While CFG 2.5 (blue) stays near the original images (black), high and low CFG scales (7.5 and 1.0) deviate fast, indicating image degradation. (c) Quantitative comparison for FID ↓ (Pokemon). CFG 2.5 achieves the most robust performance. CFG 1.0 degrades from the beginning of the chain while CFG 7.5 begins to degrade in the third iteration, which aligns with the visual inspection in (a).

still exhibit significant degradation as shown in quantitative values (FID score has been doubled in 6 iterations). Visual inspection for images is provided in Appendix C.

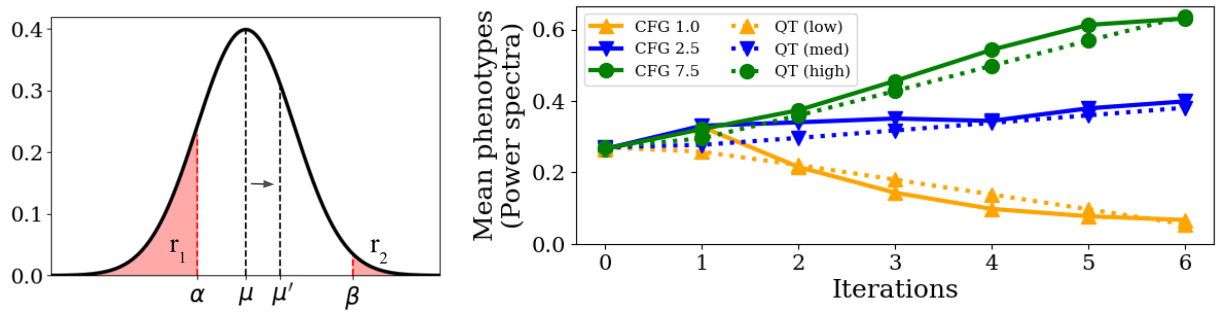
Observation 2: CFG is the most significant factor that impacts the model collapse. Throughout all our experiments, classifier-free guidance (CFG) had the biggest impact in the speed of model collapse. CFG scale was first introduced in [36] to modulate the strength between unconditional and conditional scores at each diffusion step as follows:

$$\text{Total Score} = \text{Unconditional Score} + \text{CFG} \cdot (\text{Conditional Score} - \text{Unconditional Score}). \tag{4}$$

A higher CFG means that we emphasize the conditional score for the given prompt more, which pushes the generation to align better with the prompt and often leads to higher-fidelity images. On the other hand, lower CFG places less weight on the conditional score and provides more diversity in generated images. For those familiar with temperature sampling [37], CFG plays a similar role as temperature, which adjusts the trade-off between fidelity and diversity.

In Figure 2, we observe that as we increase the CFG scale, the image quality in the first iteration improves (smaller FID_1 on x-axis), which is expected from our understanding of CFG. A more surprising part is that this comes at the cost of a worse collapse rate (an increase on the y-axis). Additionally, when the CFG scale is as high as 7.5 or 10.0, the improvement in FID_1 plateaus, and increased CFG worsens both FID_1 and collapse rate. Similarly, when the CFG scale is too low—below 2.0—the improvement in the collapse rate plateaus and both FID_1 and collapse rate begin to increase. There is an optimal region of CFG values (near 2.5, specific to Pokemon), where we achieve low collapse rate while maintaining a good quality in the first iteration as well. Moreover, Figure 3(c) presents FID for Pokemon to demonstrate how different CFG scales affect the performance during iterations. CFG scale 2.5 achieves the most robust performance for Pokemon across iterations. Interestingly, optimal CFG scales differ for different styles: 2.5 for animated or hand-writing datasets (Pokemon and Kumapi) and 1.5 for photo datasets (CelebA and Butterfly) as shown in Appendix B.

Observation 3: High CFG scales cause high-frequency degradation and low CFG scales cause low-frequency degradation. The CFG scale affects affect not only the speed of model collapse, but also the pattern of model collapse. As shown in Figure 3(a), CFG 1.0 makes the images progressively more blurry in the Chain of Diffusion, eventually collapsing to images without any structure, which we refer to as low-frequency degradation. On the other hand, for CFG 7.5 the degradation pattern looks completely different: some features start to be emphasized excessively, repetitive patterns begin to appear, and the overall color distribution becomes saturated. The t-SNE plot in Figure 3(b) clearly demonstrates that the distribution shift over iterations follows distinct paths for high, low, and medium CFG scales. These patterns were consistent in all four datasets and detailed results can be found in Appendix B. In Section 4, we detail how different patterns of power spectra in high-frequency regions from different CFG scales can be understood using the framework from genetic biology.



(a) Selection mechanism.

(b) Power spectra of images vs. Mean of phenotypes.

Figure 4: (a) **Selection mechanism with two-sided truncation.** r_1 and r_2 ratios of samples are truncated from the left and right tails, and the remaining $r = 1 - r_1 - r_2$ ratio of samples is selected. (b) **Power spectra for different CFGs (Pokemon) and quantitative trait modeling results of different selection strategies.** Directional selections with truncation can effectively explain our observations in Section 3: the behaviors of high- and low-frequency degradation and optimal CFG scale. Detailed settings are provided in Appendix D.2.

Implications of our observations. Our extensive investigations reveal that a high CFG of 7.5, a common choice to generate visually appealing images, significantly increases collapse rate to achieve slightly better FID_1. Sampling for maximizing the perceptual quality was coined as 'sampling bias' in [16]. While they reported a monotonic increase in collapse rate as CFG increased from 1.0 to 2.0, we show that the holistic picture is not entirely monotonic when we look at a wider range of CFG scales from 1.0 to 10.0. It shows an intriguing trade-off between perceptual quality and reusability. This suggests that developers concerning reusability of images can substantially improve future generations by carefully choosing CFG.

4 Quantitative Trait Models for Fully-Synthetic Training Loops

This section introduces a novel perspective for understanding the model collapse in generative models by drawing parallels between genetic biology and the Chain of Diffusion. Distinguishable iterations in the Chain of Diffusion—where each iteration is clearly separable with no duplicated individuals, and the current iteration originates from the previous one—mirror genetic processes involving successive iterations of parents and offspring. By applying quantitative trait modeling from statistical genetics, we provide a framework to describe how images evolve across iterations in the Chain of Diffusion.

We begin by introducing quantitative trait modeling and its underlying mathematical assumptions. Leveraging these assumptions, we derive a theorem demonstrating that the mean trait value exhibits linear drift while the variance stabilizes over time. We then show that this model can successfully capture the three key behaviors observed in Section 3: high-frequency degradation, low-frequency degradation, and optimal CFG scale performance. This suggests that different CFG scales in the Chain of Diffusion can be viewed as varying selection strategies, with power spectra corresponding to quantitative traits. We use the term "iteration" instead of "generation" for genetic generation to avoid confusion with image generation.

4.1 Quantitative Trait Modeling

Quantitative trait modeling in statistical genetics explores the evolution of quantitative phenotypes (e.g., height, weight, or color), which are determined by multiple genetic and environmental factors in complex ways. These phenotypes are typically assumed to follow a Gaussian distribution, with discrete iterations where parents and offspring are distinguishable (t- and $t+1$-th iterations are clearly separable).

Let the distribution of phenotypes at the t-th iteration be denoted as $\mathcal{N}(\mu_t, \sigma^2_{P,t})$ where μ_t and $\sigma^2_{P,t}$ are the mean and variance of quantitative phenotypes. The phenotypic variance $\sigma^2_{P,t}$ is the sum of the (additive) genetic variance $\sigma^2_{G,t}$ and the environmental variance σ^2_E, i.e., $\sigma^2_{P,t} = \sigma^2_{G,t} + \sigma^2_E$ [38][4]. When selection occurs in each iteration, whether natural (e.g., faster animals surviving predators) or artificial (e.g., breeding livestock for higher milk production), it affects the distribution of the effective population that influences the next iteration. We consider directional selection

[4]Genetic variance is composed of additive, dominance, and interaction variance. Here, we only consider additive variance, which is a common assumption in the field.

with truncation, as shown in Figure 4(a), where a ratio of r samples is selected by truncating r_1 from the left and r_2 from the right side of the distribution. Here, $r + r_1 + r_2 = 1$ and larger phenotype values are preferred when $r_1 > r_2$.

The (narrow-sense) heritability[5], which is defined as the proportion of phenotypic variance attributable to additive genetic factors, can also be represented using the Breeder's Eqn. [39] as:

$$h_t^2 = \frac{\sigma_{G,t}^2}{\sigma_{P,t}^2} = \frac{\sigma_{G,t}^2}{\sigma_{G,t}^2 + \sigma_E^2} = \frac{\mu_{t+1} - \mu_t}{\mu_t' - \mu_t}, \tag{5}$$

where the mean phenotype of the next iteration μ_{t+1} is represented using the mean phenotype of selected individuals μ_t', the mean phenotype of the entire population at current iteration μ_t, and heritability h_t^2. Additionally, we assume the genetic variance for the next iteration is determined by the variance of selected individuals $\sigma_{G,t+1}^2 = \sigma_{P,t}'^2$. We prove the behaviors of mean and variance of phenotypes under this setting:

Theorem 1 *Suppose the distributions of phenotypes follow Gaussian distribution and directional selection truncates individuals on both sides with ratios r_1 and r_2. Then mean of phenotypes asymptotically increases (decreases) by $\frac{c_1 c_2}{\sqrt{1-c_2}}\sigma_E$ per iteration and the variance converges to $\frac{1}{1-c_2}\sigma_E^2$ when $r_1 > r_2$ ($r_2 < r_1$), where c_1 and c_2 are constants that depend on r_1 and r_2.*

The proof of Theorem 1 is provided in Appendix D.1.

4.2 Explaining the Chain of Diffusion with Quantitative Trait Modeling

Just as phenotypes evolve through complex functions of hidden genotypes across multiple iterations in quantitative trait modeling, various continuous features of images evolve similarly during the Chain of Diffusion. A key discovery in our work is that the high-frequency power spectra are crucial phenotypes that evolve over iterations, with the CFG scales acting as different selection mechanisms. These power spectra are computed using 2D Fourier transforms, focusing on frequencies above a certain threshold to capture high-frequency components. Different CFG scales during generation correspond to different selection strategies: a high CFG selects individuals in the right tail of the distribution, favoring more detailed features with reduced diversity, while a low CFG selects from the left tail.

Figure 4(b) shows the evolution of power spectra in the Chain of Diffusion (in solid line) and the phenotype mean modeled with Equation (9) (in dotted lines). The initial mean μ_0 and genetic deviation $\sigma_{G,0}$ in the simulation are set to match those of the original image set at iteration 0. Three different configurations of ratios, r_1 and r_2, successfully model the power spectra distribution: CFG 7.5 is modeled as selecting from upper 5% of samples, CFG 2.5 selects 50% of the samples slightly favoring higher frequency, and CFG 1.0 results from selecting the lower 30%. We can see that this modeling can capture the evolution of power spectra very accurately over 6 iterations of Chain of Diffuson. Details about power spectra computation and simulation parameters are provided in Appendix D.2.2.

4.3 Statistical Genetics as a Unifying Lens to Model Collapse

Quantitative trait modeling, a tool borrowed from statistical genetics, serves as a solid theoretical framework for interpreting our experimental results. As genetic processes and the self-consuming training of generative models share a lot of similarities, we find that other concepts in mathematical genetics also have close ties to existing theoretical work on model collapse. For instance, the traditional Wright-Fisher model [19] describes how traits evolve from one generation to the next in a finite population. Due to randomness in the sampling process, the composition of traits within a finite population drifts over time and eventually collapses to a single phenotype. The Wright-Fisher model and its continuous variants [40] are exactly equivalent to the collapse behavior modeled with simple categorical or Gaussian distributions in [3, 6, 16, 22]. Given its widespread use in genetics, many extensions of the Wright-Fisher model remain an active area of research, such as including different mechanisms of selection [41, 42] or mutations [43]. Beyond the current work and existing theoretical studies on model collapse, we believe that statistical genetics offers a unified perspective to understand model collapse by reducing the complex dynamics of the self-consuming loop of generative model training to a small number of parameters, from which we can gain valuable insights.

5 Reusable Image Generation with ReDiFine

In the previous sections, we have discovered a significant role of CFG in model collapse and that an appropriate choice of CFG can effectively mitigate the collapse. However, the optimal CFG value that minimizes the collapse rate is

[5]The heritability is narrow-sense when the genetic variance is restricted to additive variance.

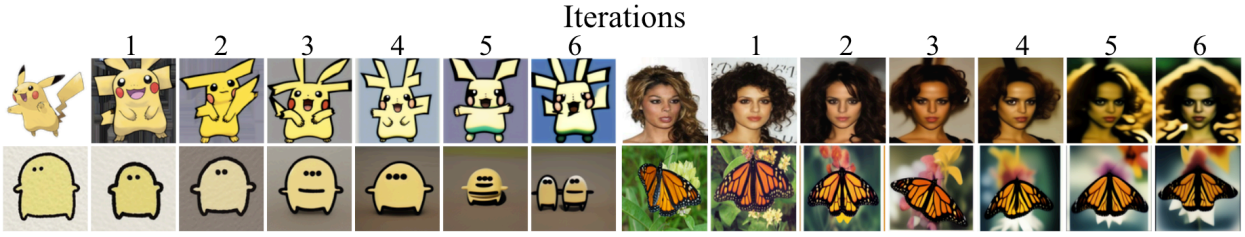


Figure 5: **ReDiFine effectively mitigates image degradation in the Chain of Diffusion.** ReDiFine successfully preserves the characteristics and features without further dataset-specific hyperparameter search. Artifacts observed in high-frequency degradation do not exist for all four datasets.

different for each dataset (e.g., CFG 1.5 for CelebA, CFG 2.5 for Pokemon). There is no efficient way of finding an optimal CFG other than performing a grid search over a wide range of values and iteratively fine-tuning the diffusion model to evaluate the collapse rate for each configuration. In practical scenarios, it is unlikely that end users who are not machine learning experts will go through such a process during finetuning, just to prevent a potential model collapse that can happen in the next generation. This raises the question: *How can we design a finetuning and generation strategy that is user-friendly and can effectively slow down model collapse?*

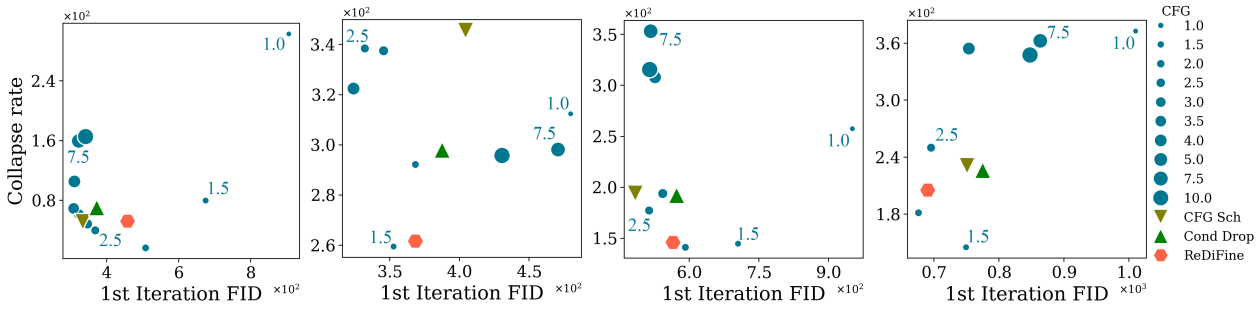
To address this question, we again draw inspiration from the evolution process in nature. In biology, mutations naturally counteract genetic drift and preserve diversity. Furthermore, selection in nature is often a soft process rather than a hard truncation, as illustrated in Figure 4(a). This soft selection allows for the inclusion of outliers, thereby maintaining the overall genetic diversity. We connect these biological inspirations with two strategies: *condition drop finetuning* to introduce more randomness and *CFG scheduling* during generation to transform hard selection to a softer one[6]. We propose **Re**usable **Di**ffusion **Fine**tuning (ReDiFine) method that incorporates these two ideas and show that it is highly effective at mitigating model collapse without the need for any finetuning.

Condition drop finetuning. We introduce condition drop finetuning, which randomly drops the text condition during finetuning to update both the conditional and unconditional scores. Although condition drop was suggested in the original CFG paper [36], it is not a common practice during finetuning since we can achieve good images without it in the first iteration where model collapse is yet to happen (see Figure 1(b)). However, the small Diff ($=$ Cond Score $-$ Uncond Score) can accumulate over multiple iterations, leading to a significant gap as the Chain of Diffusion progresses. On the other hand, condition drop finetuning with drop probability 0.2 preserves the norm of Diff over the iterations (see Figure 33(b)).

CFG Scheduling. We propose gradually reducing the CFG scale during diffusion steps to mitigate the impacts of overemphasizing the conditional score in later stages, which can lead to high-frequency degradation. Specifically, we exponentially decrease the CFG scale s during T diffusion steps as $s = s_0 \times e^{-\alpha \times t/T}$, where s_0 is the initial CFG scale and α is the rate of exponential decay. This scheduling approach is consistent with findings by [44], which suggest that different diffusion steps contribute uniquely to the generation process. High CFG lets us capture high-level semantic information accurately during the initial diffusion steps while lower CFG in later steps can prevent generating unnecessary high-frequency details.

ReDeFine Results. We present the generated images and quantitative metrics for ReDiFine. We use the initial CFG scale $s_0 = 7.5$, diffusion steps $T = 30$, decay rate $\alpha = 2$, and condition drop probability 0.2 for all of our experiments, except in the robustness comparison and ablation study. While ReDiFine can be further optimized through hyperparameter tuning (e.g., changing condition drop probability), our goal is to demonstrate that ReDiFine robustly mitigates model collapse with these default parameter settings for all datasets. In Figure 5, we can clearly see that ReDiFine significantly improves the image quality at later iterations compared to the baseline (Figure 1(b)) for all four datasets. In addition to the visual comparison, Figure 6 quantitatively shows the collapse-FID trade-off of ReDiFine. In all four datasets, ReDiFine shows substantially lower collapse rate (y-axis), compared to the baseline case (CFG=7.5). Furthermore, the performance of ReDiFine is close to the optimal Pareto curve spanned by different CFG scales, achieving similar performance as the optimal CFG values across all four datasets, demonstrating its effectiveness as a universal solution for mitigating model collapse. In contrast, using a fixed CFG scale that works well for one dataset often fails on others: CFG 2.5 is optimal for Pokemon but performs poorly for CelebA-1k and Butterfly, and CFG 1.5 is optimal for CelebA but performs poorly for Pokemon and Kumapi.

[6]We show a modified quantitative trait modeling result with these two modifications in Appendix D.2 and show that it captures the ReDiFine experimental results effectively. In this section, we focus on showing the image generation results with ReDiFine. We refer the curious readers to the appendix.



(a) Pokemon. (b) CelebA-1k. (c) Kumapi. (d) Butterfly.

Figure 6: **ReDiFine effectively mitigates collapse-FID trade-off across all four datasets**. While the optimal CFG scale varies for different datasets, ReDiFine consistently achieves low collapse rate and FID at the same time (lower is better). Note that the differences in FID are relatively smaller than those in collapse rate, supporting the necessity to evaluate collapse rate in the Chain of Diffusion.



Figure 7: **Comparison of ReDiFine and baseline (CFG scale 7.5) with training sets mixed with original and synthetic images from the previous iteration.** While mixing real images as much as 90% still results in model collapse for the baseline (as shown in the first row), the ability of ReDiFine to mitigate model collapse is even more highlighted by mixing real images (second row).

We also compare ReDiFine with real image mixing, which is suggested as a mitigation strategy in several previous papers [3, 8, 16, 23]. In Figure 7, we can observe that even infusing the dataset with 90% real images, it shows severe image degradation within six iterations. By visual comparison, we can see that Pikachu images in Figure 5 have less degradation than those with real image mixing. Furthermore, applying ReDiFine to these mixed datasets, as shown in Figure 7, significantly improves image quality compared to the baseline. This demonstrates that ReDiFine is an effective solution for various settings and can be used alongside other mitigation strategies such as real data mixing.

Ablation study & Further analyses. We conducted an ablation study to understand the contributions of condition drop finetuning and CFG scheduling to the success of ReDiFine. We plot the results of using only condition drop and CFG scheduling in green triangles on Figure 6. In Pokemon, using only one of those strategies outperforms ReDiFine, but in all other datasets, using only one strategy shows higher collapse rate than ReDiFine. Especially in CelebA, using either one of them showed significantly worse performance than ReDiFine. These results suggest that combining both condition drop and CFG scheduling builds robustness to the method, making ReDiFine effective across all tested datasets. We conducted further analyses on ReDiFine, examining the distribution of latent features, the evolution of the norm of Diff, the power spectra using 2D Fourier transforms, and forensic fingerprints based on prior studies [45, 46]. Our analysis shows that ReDiFine effectively preserves the latent distribution and the norms of Diff over six iterations, with forensic fingerprints closely resembling those of the optimal CFG case. Detailed results are provided in Appendix G.

Reusable image generation as a responsible AI practice. In this section, we demonstrated that ReDiFine significantly slows the collapse rate without sacrificing image quality, similar to how fair classifiers reduce bias without compromising accuracy [47]. Adopting ReDiFine is a responsible, environment-conscious practice to prevent polluting the world with images that might look visually appealing, but totally unusable to improve future AI models.

6 Conclusion

The influx of AI-generated data into the world is inevitable and training sets that consist of synthetic data will be part of the AI development pipeline. In this paper, we empirically and theoretically studied the scenario of finetuning a model with its own generated data, where a gradual degradation called "model collapse" happens. We (1) identify the most

impactful factor through comprehensive empirical investigations, (2) develop a novel theoretical perspective inspired by statistical genetics to explain model collapse, and (3) propose an effective mitigation strategy that generates reusable images for future training.

We started this paper with a question: can current AI models learn from their own output and improve themselves? Our paper shows a glimpse that widely-used text-to-image models are not ready to improve from their own creation quite yet. While we presented one solution focused on generating *reusable data*, many open directions remain, such as developing algorithms that can distinguish between real and synthetic data and apply different learning techniques accordingly.

References

[1] Jiaxin Huang, Shixiang Shane Gu, Le Hou, Yuexin Wu, Xuezhi Wang, Hongkun Yu, and Jiawei Han. Large language models can self-improve. *arXiv preprint arXiv:2210.11610*, 2022.

[2] Matthias Gerstgrasser, Rylan Schaeffer, Apratim Dey, Rafael Rafailov, Henry Sleight, John Hughes, Tomasz Korbak, Rajashree Agrawal, Dhruv Pai, Andrey Gromov, et al. Is model collapse inevitable? breaking the curse of recursion by accumulating real and synthetic data. *arXiv preprint arXiv:2404.01413*, 2024.

[3] Quentin Bertrand, Avishek Joey Bose, Alexandre Duplessis, Marco Jiralerspong, and Gauthier Gidel. On the stability of iterative retraining of generative models on their own data. *arXiv preprint arXiv:2310.00429*, 2023.

[4] Nate Gillman, Michael Freeman, Daksh Aggarwal, Chia-Hong Hsu, Calvin Luo, Yonglong Tian, and Chen Sun. Self-Correcting Self-Consuming Loops for Generative Model Training, April 2024. arXiv:2402.07087 [cs, stat].

[5] Rohan Taori and Tatsunori Hashimoto. Data feedback loops: Model-driven amplification of dataset biases. In *International Conference on Machine Learning*, pages 33883–33920. PMLR, 2023.

[6] Ilia Shumailov, Zakhar Shumaylov, Yiren Zhao, Yarin Gal, Nicolas Papernot, and Ross Anderson. The curse of recursion: Training on generated data makes models forget. *arXiv preprint arXiv:2305.17493*, 2023.

[7] Elvis Dohmatob, Yunzhen Feng, and Julia Kempe. Model Collapse Demystified: The Case of Regression, April 2024. arXiv:2402.07712 [cs, stat].

[8] Shi Fu, Sen Zhang, Yingjie Wang, Xinmei Tian, and Dacheng Tao. Towards theoretical understandings of self-consuming generative models. *arXiv preprint arXiv:2402.11778*, 2024.

[9] Matteo Marchi, Stefano Soatto, Pratik Chaudhari, and Paulo Tabuada. Heat death of generative models in closed-loop learning. *arXiv preprint arXiv:2404.02325*, 2024.

[10] Gonzalo Martínez, Lauren Watson, Pedro Reviriego, José Alberto Hernández, Marc Juarez, and Rik Sarkar. Towards understanding the interplay of generative artificial intelligence and the internet. In *International Workshop on Epistemic Uncertainty in Artificial Intelligence*, pages 59–73. Springer, 2023.

[11] Elvis Dohmatob, Yunzhen Feng, Pu Yang, Francois Charton, and Julia Kempe. A tale of tails: Model collapse as a change of scaling laws. *arXiv preprint arXiv:2402.07043*, 2024.

[12] Yanzhu Guo, Guokan Shang, Michalis Vazirgiannis, and Chloé Clavel. The Curious Decline of Linguistic Diversity: Training Language Models on Synthetic Text, April 2024. arXiv:2311.09807 [cs].

[13] Martin Briesch, Dominik Sobania, and Franz Rothlauf. Large language models suffer from their own output: An analysis of the self-consuming training loop. *arXiv preprint arXiv:2311.16822*, 2023.

[14] Matyas Bohacek and Hany Farid. Nepotistically trained generative-ai models collapse. *arXiv preprint arXiv:2311.12202*, 2023.

[15] Gonzalo Martínez, Lauren Watson, Pedro Reviriego, José Alberto Hernández, Marc Juarez, and Rik Sarkar. Combining generative artificial intelligence (ai) and the internet: Heading towards evolution or degradation? *arXiv preprint arXiv:2303.01255*, 2023.

[16] Sina Alemohammad, Josue Casco-Rodriguez, Lorenzo Luzi, Ahmed Imtiaz Humayun, Hossein Babaei, Daniel LeJeune, Ali Siahkoohi, and Richard G Baraniuk. Self-consuming generative models go mad. *arXiv preprint arXiv:2307.01850*, 2023.

[17] Ryuichiro Hataya, Han Bao, and Hiromi Arai. Will Large-scale Generative Models Corrupt Future Datasets? In *2023 IEEE/CVF International Conference on Computer Vision (ICCV)*, pages 20498–20508, Paris, France, October 2023. IEEE.

[18] Ronald Aylmer Fisher. *The genetical theory of natural selection: a complete variorum edition*. Oxford University Press, 1999.

[19] Sewall Wright. Evolution in mendelian populations. *Genetics*, 16(2):97, 1931.

[20] Motoo Kimura. Solution of a process of random genetic drift with a continuous model. *Proceedings of the National Academy of Sciences*, 41(3):144–150, 1955.

[21] Cyriel Paris, Bertrand Servin, and Simon Boitard. Inference of selection from genetic time series using various parametric approximations to the wright-fisher model. *G3: Genes, Genomes, Genetics*, 9(12):4073–4086, 2019.

[22] Ilia Shumailov, Zakhar Shumaylov, Yiren Zhao, Nicolas Papernot, Ross Anderson, and Yarin Gal. Ai models collapse when trained on recursively generated data. *Nature*, 631(8022):755–759, 2024.

[23] Damien Ferbach, Quentin Bertrand, Avishek Joey Bose, and Gauthier Gidel. Self-consuming generative models with curated data provably optimize human preferences. *arXiv preprint arXiv:2407.09499*, 2024.

[24] Robin Rombach, Andreas Blattmann, Dominik Lorenz, Patrick Esser, and Björn Ommer. High-resolution image synthesis with latent diffusion models. In *Proceedings of the IEEE/CVF conference on computer vision and pattern recognition*, pages 10684–10695, 2022.

[25] Edward J Hu, Yelong Shen, Phillip Wallis, Zeyuan Allen-Zhu, Yuanzhi Li, Shean Wang, Lu Wang, and Weizhu Chen. Lora: Low-rank adaptation of large language models. *arXiv preprint arXiv:2106.09685*, 2021.

[26] kohya-ss. kohya-ss trainer.

[27] Pokémon. Pokédex. `https://www.pokemon.com/us/pokedex`, 2023. Accessed: 2023-04-19.

[28] Ihelon. Illustrations kumapi390, 2022. Accessed: 2023-04-19.

[29] Veeralakrishna. Butterfly dataset. `https://www.kaggle.com/datasets/veeralakrishna/butterfly-dataset`, 2020. Accessed: 2024-01-03.

[30] Ziwei Liu, Ping Luo, Xiaogang Wang, and Xiaoou Tang. Deep learning face attributes in the wild. In *Proceedings of International Conference on Computer Vision (ICCV)*, December 2015.

[31] Martin Heusel, Hubert Ramsauer, Thomas Unterthiner, Bernhard Nessler, and Sepp Hochreiter. Gans trained by a two time-scale update rule converge to a local nash equilibrium. *Advances in neural information processing systems*, 30, 2017.

[32] George Stein, Jesse Cresswell, Rasa Hosseinzadeh, Yi Sui, Brendan Ross, Valentin Villecroze, Zhaoyan Liu, Anthony L Caterini, Eric Taylor, and Gabriel Loaiza-Ganem. Exposing flaws of generative model evaluation metrics and their unfair treatment of diffusion models. *Advances in Neural Information Processing Systems*, 36, 2024.

[33] Maxime Oquab, Timothée Darcet, Théo Moutakanni, Huy Vo, Marc Szafraniec, Vasil Khalidov, Pierre Fernandez, Daniel Haziza, Francisco Massa, Alaaeldin El-Nouby, et al. Dinov2: Learning robust visual features without supervision. *arXiv preprint arXiv:2304.07193*, 2023.

[34] Christian Szegedy, Vincent Vanhoucke, Sergey Ioffe, Jon Shlens, and Zbigniew Wojna. Rethinking the inception architecture for computer vision. In *Proceedings of the IEEE conference on computer vision and pattern recognition*, pages 2818–2826, 2016.

[35] Alec Radford, Jong Wook Kim, Chris Hallacy, Aditya Ramesh, Gabriel Goh, Sandhini Agarwal, Girish Sastry, Amanda Askell, Pamela Mishkin, Jack Clark, Gretchen Krueger, and Ilya Sutskever. Learning transferable visual models from natural language supervision, 2021.

[36] Jonathan Ho and Tim Salimans. Classifier-free diffusion guidance. *arXiv preprint arXiv:2207.12598*, 2022.

[37] David H Ackley, Geoffrey E Hinton, and Terrence J Sejnowski. A learning algorithm for boltzmann machines. *Cognitive science*, 9(1):147–169, 1985.

[38] DS Falconer. *Introduction to quantitative genetics*. Pearson Education India, 1996.

[39] Jay L Lush. *Animal breeding plans*. Read Books Ltd, 2013.

[40] Paula Tataru, Maria Simonsen, Thomas Bataillon, and Asger Hobolth. Statistical inference in the wright–fisher model using allele frequency data. *Systematic biology*, 66(1):e30–e46, 2017.

[41] Zhangyi He, Mark Beaumont, and Feng Yu. Effects of the ordering of natural selection and population regulation mechanisms on wright-fisher models. *G3: Genes, Genomes, Genetics*, 7(7):2095–2106, 2017.

[42] Ingemar Kaj, Carina F Mugal, and Rebekka Müller-Widmann. A wright–fisher graph model and the impact of directional selection on genetic variation. *Theoretical Population Biology*, 159:13–24, 2024.

[43] Brian Charlesworth. How long does it take to fix a favorable mutation, and why should we care? *The American Naturalist*, 195(5):753–771, 2020.

[44] Yogesh Balaji, Seungjun Nah, Xun Huang, Arash Vahdat, Jiaming Song, Qinsheng Zhang, Karsten Kreis, Miika Aittala, Timo Aila, Samuli Laine, et al. ediff-i: Text-to-image diffusion models with an ensemble of expert denoisers. *arXiv preprint arXiv:2211.01324*, 2022.

[45] Riccardo Corvi, Davide Cozzolino, Giovanni Poggi, Koki Nagano, and Luisa Verdoliva. Intriguing properties of synthetic images: from generative adversarial networks to diffusion models. In *Proceedings of the IEEE/CVF Conference on Computer Vision and Pattern Recognition*, pages 973–982, 2023.

[46] Riccardo Corvi, Davide Cozzolino, Giada Zingarini, Giovanni Poggi, Koki Nagano, and Luisa Verdoliva. On the detection of synthetic images generated by diffusion models. In *ICASSP 2023-2023 IEEE International Conference on Acoustics, Speech and Signal Processing (ICASSP)*, pages 1–5. IEEE, 2023.

[47] Wael Alghamdi, Hsiang Hsu, Haewon Jeong, Hao Wang, Peter Michalak, Shahab Asoodeh, and Flavio Calmon. Beyond adult and compas: Fair multi-class prediction via information projection. *Advances in Neural Information Processing Systems*, 35:38747–38760, 2022.

[48] StabilityAI. Sd vae ft mse original, 2022. Accessed: 2023-04-19.

[49] Jason Ansel, Edward Yang, Horace He, Natalia Gimelshein, Animesh Jain, Michael Voznesensky, Bin Bao, Peter Bell, David Berard, Evgeni Burovski, Geeta Chauhan, Anjali Chourdia, Will Constable, Alban Desmaison, Zachary DeVito, Elias Ellison, Will Feng, Jiong Gong, Michael Gschwind, Brian Hirsh, Sherlock Huang, Kshiteej Kalambarkar, Laurent Kirsch, Michael Lazos, Mario Lezcano, Yanbo Liang, Jason Liang, Yinghai Lu, CK Luk, Bert Maher, Yunjie Pan, Christian Puhrsch, Matthias Reso, Mark Saroufim, Marcos Yukio Siraichi, Helen Suk, Michael Suo, Phil Tillet, Eikan Wang, Xiaodong Wang, William Wen, Shunting Zhang, Xu Zhao, Keren Zhou, Richard Zou, Ajit Mathews, Gregory Chanan, Peng Wu, and Soumith Chintala. PyTorch 2: Faster Machine Learning Through Dynamic Python Bytecode Transformation and Graph Compilation. In *29th ACM International Conference on Architectural Support for Programming Languages and Operating Systems, Volume 2 (ASPLOS '24)*. ACM, April 2024.

[50] Junnan Li, Dongxu Li, Caiming Xiong, and Steven Hoi. Blip: Bootstrapping language-image pre-training for unified vision-language understanding and generation, 2022.

[51] Hakurei. Waifu diffusion v1.4. `https://huggingface.co/hakurei/waifu-diffusion-v1-4`, 2022. Accessed: 2023-04-18.

Supplementary Material

A Experimental setup

A.1 Hyperparameters

We finetune Stable Diffusion v1.5 [24] using LoRA [25] at each iteration, with ft-MSE [48] as a fixed VAE to project images into latent space. Horizontal flip is the only image augmentation applied. Our implementation follows [26] and is built on PyTorch v2.2.2 [49], with torchvision 0.17.2, running on CUDA 12.4 using NVIDIA A-100 and L40S GPUs. All default hyperparameters are listed in Table 1.

Table 1: Default hyperparameters used for the Chain of Diffusion.

Hyperparameter	**Value**
Optimizer	AdamW
Learning Rate - Unet	0.0001
Learning Rate - CLIP	0.00005
LoRA Weight Scaling	8
LoRA Rank	32
Batch Size	6
Max Epochs	100
CLIP Skip	2
Noise Offset	0.0
Mixed Precision	fp16
Loss Function	MSE
Min SNR gamma	5.0
Max Gradient Norm Clipping	1.0
Caption Dropout Rate	0.0
Sampler	Euler A
Classifier-Free Guidance Scale	7.5
Number of Diffusion Steps	30
Number of Images per Prompt	1

A.2 Datasets

We use four image datasets to demonstrate the universal nature of degradation: Pokemon [27], Kumapi [28], Butterfly [29], and CelebA-1k [30], covering animation, handwriting, and real images. All images are resized to 512×512 pixels. Text prompts are generated using BLIP captioner [50] and Waifu Diffusion v1.4 tagger [51]. Sample images and prompts can listed in Table 2.

Pokemon. The Pokemon dataset [27] contains 1008 images indexed by number, with prompts combining BLIP captions (length 50-75 words) and Waifu Diffusion tagger.

CelebA-1k. CelebA-1k is a subsample of 1000 images from CelebA [30], with BLIP captions (25-50 words).

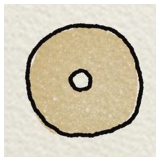
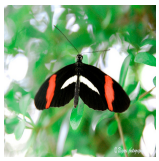
Kumapi. Kumapi [28] includes 391 handwriting-style images, with Waifu-generated prompts and manual adjustments.

Butterfly. Butterfly [29] includes 832 images across 8 species, using BLIP captions (length 50-75 words) and species descriptions.

B Different CFG Scales

This section presents images from Chain of Diffusion at various CFG scales for the four datasets. Figure 8, 9, 10, and 11 corresponds to Pokemon, CelebA-1k, Kumapi, and Butterfly, respectively. Each dataset shows results for five CFG scales, covering high, medium, and low values. The optimal medium CFG scale is 2.5 for Pokemon and Kumapi, and 1.5 for CelebA-1k and Butterfly. Lower-than-optimal CFG scales lead to low-frequency degradations,

Table 2: Sample images and prompts for Pokemon, CelebA-1k, Kumapi, and Butterfly datasets.

Pokemon	
a green pokemon with red eyes and a leaf on the back of its head and tail, an image of the pokemon character with a red eye and big green tail, all set up to look like it is holding a lea, ultra-detailed, high-definition, high quality, masterpiece, sugimori ken (style), solo, smile, open mouth, simple background, red eyes, white background, standing, full body, pokemon (creature), no humans, fangs, transparent background, claws, Bulbasaur	
a very cute looking pokemon with a big leaf on its back and a big leaf on its head, a very cute little pokemon character with leaves in the back ground around his chest and hea, white background, ultra-detailed, high-definition, high quality, masterpiece, sugimori ken (style), solo, red eyes, closed mouth, standing, full body, pokemon (creature), no humans, fangs, transparent background, claws, outline, white outline, animal focus, fangs out	
CelebA-1k	
a woman with brown hair smiling and posing for a picture in front of a mirror and gold and white stripes	
a woman with a very long red hair smiles and laughs on a city street and other people in the background	
Kumapi	
solo, simple background, food, donut, grey background, no humans, food focus, still life, Kumapi style	
solo, looking at viewer, cute yellow figure, two tiny hands and feet, simple background, black dot eyes, white background, grey background, no humans, Kumapi style	
Butterfly	
a crimson patched longwing butterfly with a red and black stripe on its wings, wings are long, narrow, rounded, black, crossed on fore wing by broad crimson patch, and on hind wing by narrow yellow line	
a Common Buckeye butterfly is sitting on a flower in the sun, wings scalloped and rounded except at drawn-out fore wing tip, on hind wing, 1 large eyespot near upper margin and 1 small eyespot below it. Eyespots are black, yellow-rimmed, with iridescent blue and lilac irises, on fore wing, 1 very small near tip and 1 large eyespot in white fore wing bar.	

while higher-than-optimal scales result in high-frequency degradations with saturated colors and repetitive patterns. Notably, the optimal CFG for Pokemon and Kumapi causes severe degradation in CelebA-1k and Butterfly.

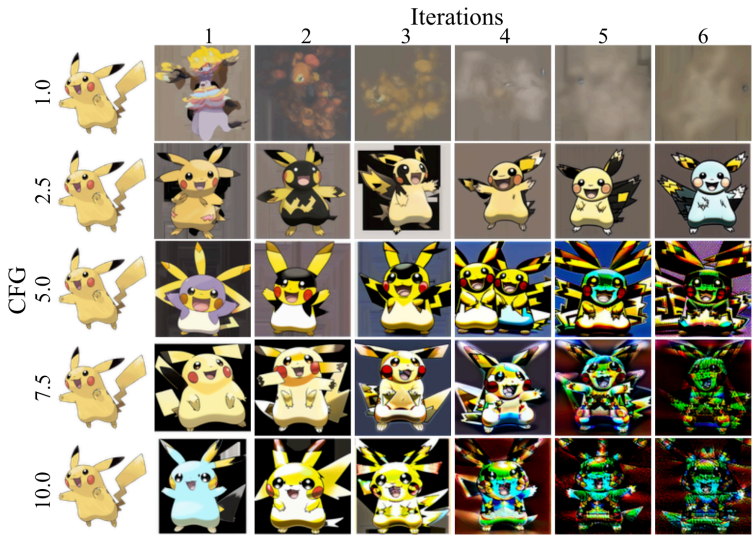


Figure 8: Chain of Diffusion for Pokemon at various CFG scales. The optimal CFG scale is 2.5.

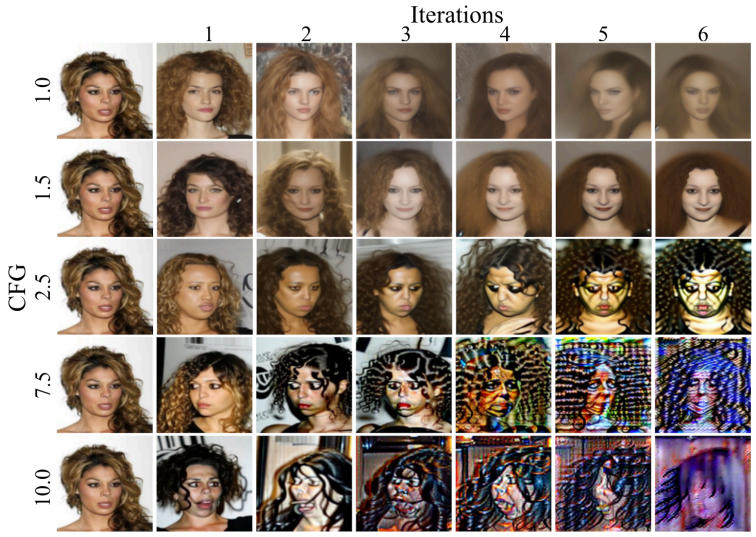


Figure 9: Chain of Diffusion for CelebA-1k at various CFG scales. The optimal CFG scale is 1.5.

C Hyperparameter investigations to unveil the most significant factor of degradation

This section presents experimental results identifying the most significant factors contributing to degradation in the Chain of Diffusion. We systematically vary each hyperparameter from Figure 2, using the default settings from Table 1, to assess their impact on degradation. The CFG scale is fixed at 7.5 for all cases.

C.1 Training set size

We used CelebA dataset [30] to examine how training set size (both D_0 and D_k) impacts degradation in the Chain of Diffusion. By subsampling, we adjusted the training set to 100, 250, 500, and 2000 images. Degradation occurs regardless of dataset size, as shown in Figure 12, but appears earlier with smaller sets. By the 6th iteration, images degrade severely for all cases. The number of parameter updates was kept constant across all dataset sizes.

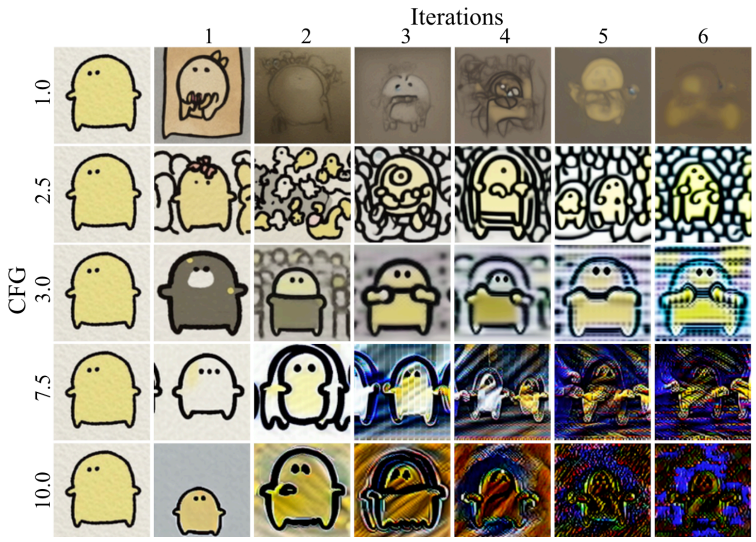


Figure 10: Chain of Diffusion for Kumapi at various CFG scales. The optimal CFG scale is 2.5.

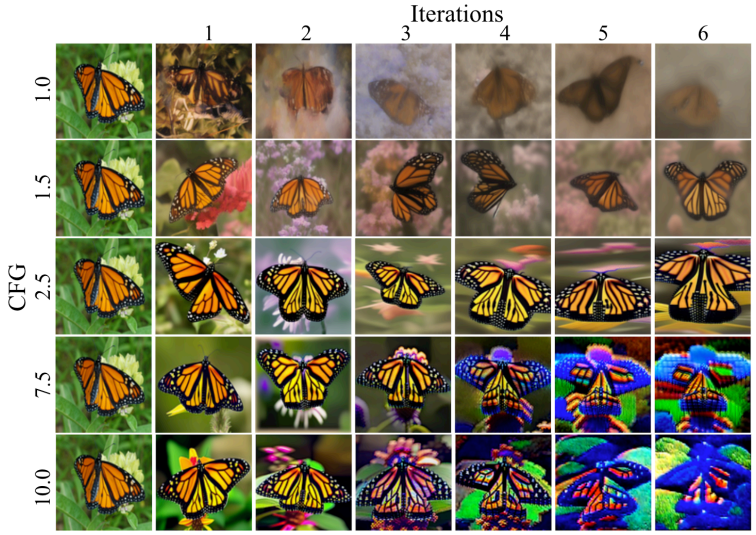


Figure 11: Chain of Diffusion for Butterfly at various CFG scales. The optimal CFG scale is 1.5.

C.2 Number of images per prompt

Generating multiple images per prompt is a simple way to increase training set diversity and can be considered as a solution to mitigate degradation in the Chain of Diffusion. We tested this by generating 5 times more images. As shown in Figure 13, while degradation is slightly delayed (by one iteration), it remains unmitigated, and the high computational cost makes this approach impractical.

C.3 Mixing real images to synthetic sets

Many previous works suggest augmenting the training set with real images to mitigate degradation during iterative training. We investigated whether mixing images from the original training set into the synthetic set at each iteration could alleviate this issue. At each iteration, images are randomly replaced with corresponding real images. Figure 14 and 15 show how degradation in the Chain of Diffusion varies when 50% and 90% of images are replaced for Pokemon and CelebA-1k datasets, respectively. Notably, even 10% synthetic images are sufficient to induce degradation, and 50% replacement rarely slows it down. CelebA-1k dataset appears to be significantly more susceptible to degradation.

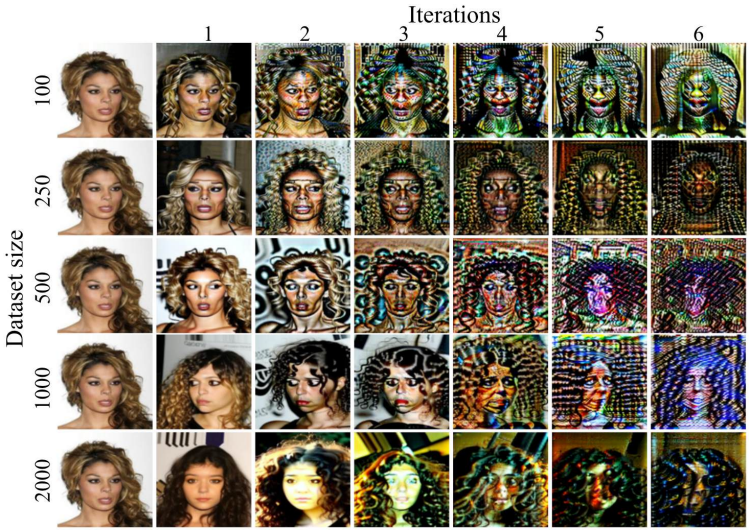


Figure 12: Chain of Diffusion on CelebA dataset with varying training set sizes. Degradation occurs faster with smaller sets, but all result in severe degradation by the 6th iteration.



Figure 13: Chain of Diffusion on Pokemon dataset with multiple images generated per prompt. Increasing the training set size in this way does not mitigate degradation.

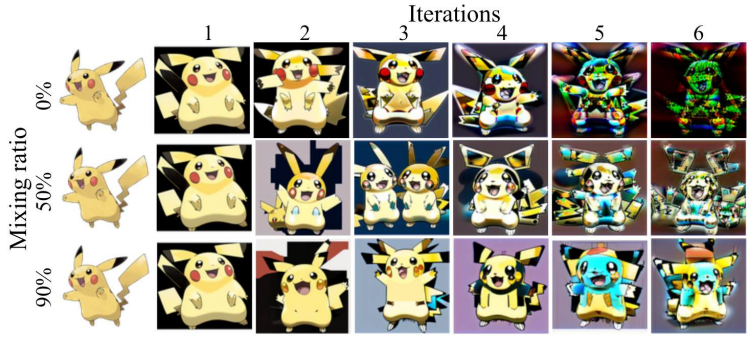


Figure 14: Chain of Diffusion on Pokemon dataset with real images randomly replacing synthetic images at each iteration. A 50% replacement rarely slows degradation, while 10% synthetic images are sufficient to initiate it.

C.4 Prompt Set

We hypothesized that the descriptiveness of prompts influences degradation in the Chain of Diffusion. We tested various prompt sets for Pokemon and CelebA-1k datasets. For Pokemon dataset, the default prompt set consists of concatenated Waifu and BLIP captions, with BLIP captions ranging from 50 to 75 words. Figure 16 shows how using only Waifu prompts and varying BLIP caption lengths affect degradation. Notably, different styles of high-frequency degradation were observed; shorter prompts reduced repetitive patterns but decreased diversity. In CelebA-1k dataset, varying BLIP caption lengths resulted in similar degradation levels, but prompts that were either insufficiently or excessively descriptive caused the images to deviate from the originals, as shown in Figure 17.

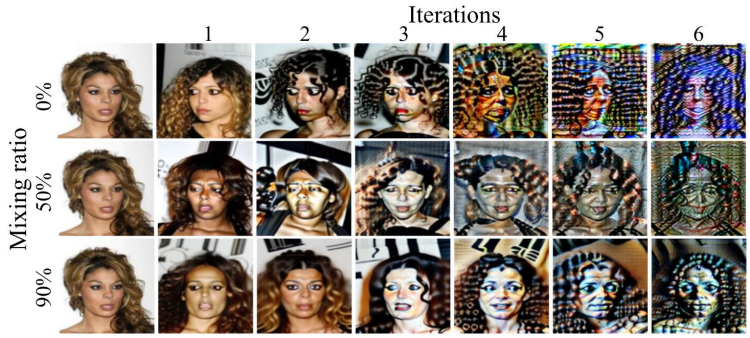


Figure 15: Chain of Diffusion on CelebA-1k dataset with real images randomly replacing synthetic images at each iteration. A 50% replacement rarely slows degradation, while 10% synthetic images are sufficient to initiate it. It suffers from more severe degradation than Pokemon dataset as compared with Figure 14.

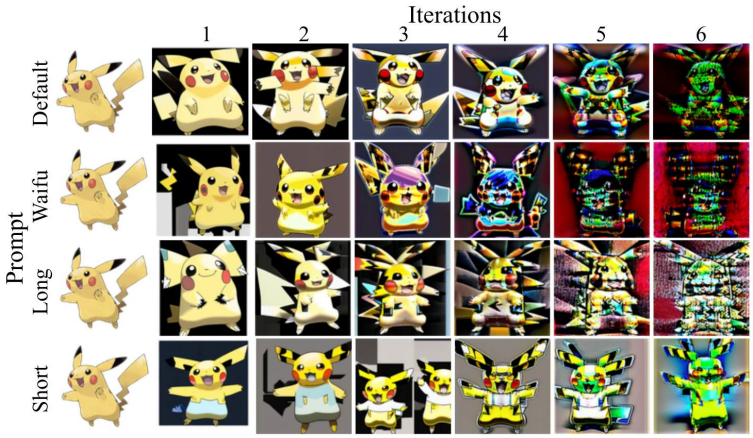


Figure 16: Chain of Diffusion on Pokemon dataset with different prompts. The default prompts are concatenations of BLIP captions (50-75 words) and Waifu captions. We compare the Chain of Diffusion using default captions, Waifu captions, short (less than 25 words) and long (50-75 words) BLIP captions.

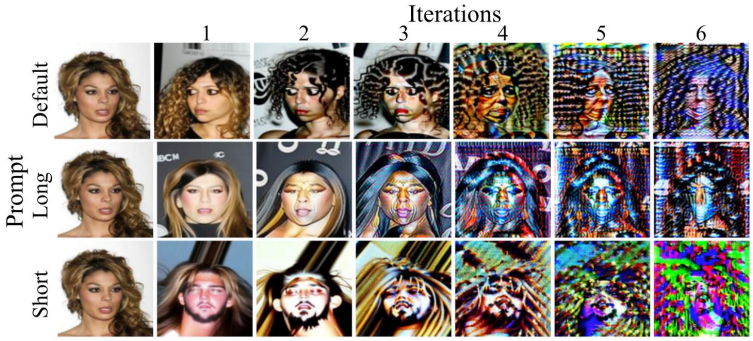


Figure 17: Chain of Diffusion on CelebA-1k dataset with different prompts. The default prompts range from 25 to 50 words. We compare the Chain of Diffusion using longer prompts (over 50 words) and shorter prompts (under 25 words).

C.5 U-Net and Text-Encoder

Figure 18 illustrates the Chain of Diffusion with either the U-Net or text encoder finetuned. When the text encoder is not updated (second row), similar degradation occurs. However, the degradation pattern changes when the U-Net is not updated, as the model's ability to generate images remains unchanged. In contrast, updating the text encoder results in a loss of image content preservation.

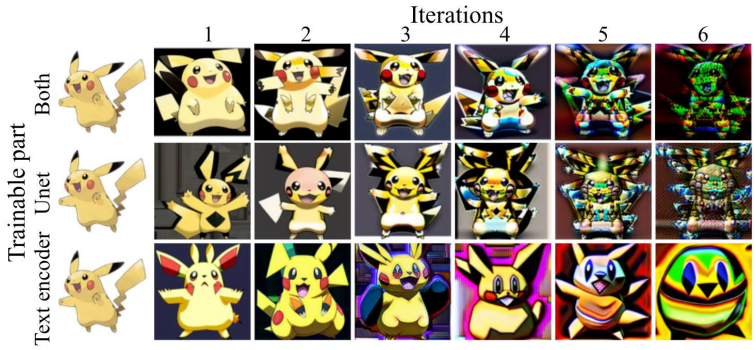


Figure 18: Chain of Diffusion on Pokemon dataset with either the U-Net or text encoder finetuned.

C.6 Number of diffusion steps

We investigated whether an insufficient number of diffusion steps during generation contributes to degradation. Figure 19 shows that increasing the number of diffusion steps does not enhance the Chain of Diffusion.

C.7 Number of Epochs

We also examined whether insufficient or excessive training affects our default setting. As shown in Figure 19, images from the initial iterations exhibit similar quality, resulting in comparable degradations. We set the default finetuning to 100 epochs since loss values continue to decrease after 50 epochs.

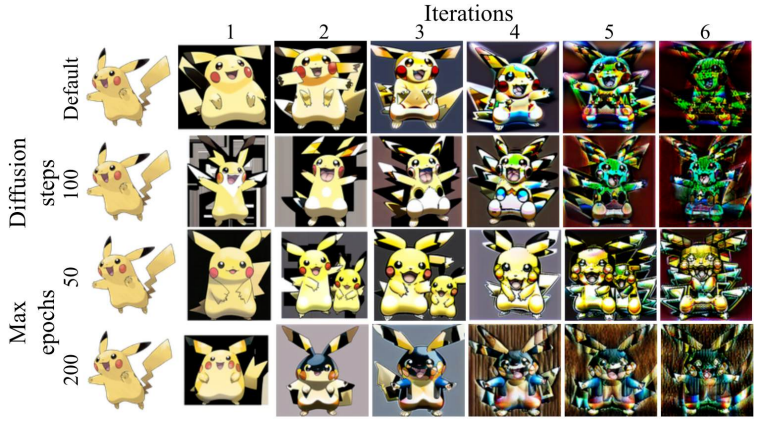


Figure 19: Chain of Diffusion on Pokemon dataset with varying diffusion steps and training epochs. Both increased diffusion steps and differing training epochs fail to mitigate degradation, resulting in similar patterns.

C.8 Learning Rate

Similarly, we assessed finetuning adequacy in Figure 20 by adjusting the learning rates for the U-Net and text encoder by x10 and x0.1. Images from the initial iterations show that the default values are suitable for finetuning. Although the styles are different, degradation consistently occurs across different learning rates.

C.9 CLIP Skip

We investigated the impact of the CLIP skip hyperparameter on degradation. The CLIP skip determines which intermediate feature from the CLIP text encoder is used as the text embedding for conditional generation, with smaller values selecting features closer to the output and larger values selecting those nearer to the input text. As shown in Figure 21, this hyperparameter has minimal effect on degradation patterns.

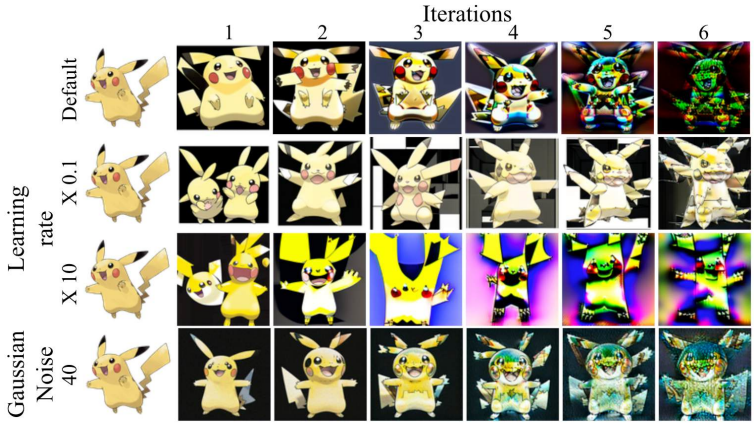


Figure 20: Chain of Diffusion on Pokemon dataset with varying learning rates and added Gaussian noise to the original training set.

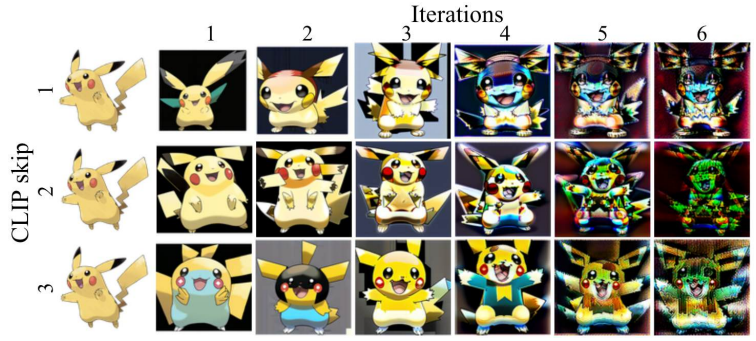


Figure 21: Chain of Diffusion on Pokemon dataset using different CLIP skip hyperparameters. The CLIP skip hyperparameter shows a negligible effect on degradation.

C.10 Adding Gaussian noise to the original training set

We examined whether differences between real and synthetic images contribute to degradation by adding random Gaussian noise to the original training set D_0. Figure 20 illustrates that while the characteristics of the original training set have some effect, degradation still occurs. This supports our findings that degradations are universal across real, animation, and handwritten images.

C.11 Stable Diffusion XL

We investigated image degradation for a different Stable Diffusion model, noting that the optimal hyperparameters for finetuning SDXL using LoRA are not well established. Consequently, we applied the same hyperparameters used for Stable Diffusion v1.5, which may be suboptimal. To manage space complexity, we reduced the batch size to 2 and maintained a resolution of 512×512, as the first iteration images exhibit impressive quality. Results are presented in Figure 22.

D Quantitative Trait Modeling

D.1 Proof of Theorem 1

Proof. The difference between the successive means in quantitative trait modeling is given by:

$$\Delta\mu_t = \mu_{t+1} - \mu_t = h_t^2(\mu_t' - \mu_t). \tag{6}$$

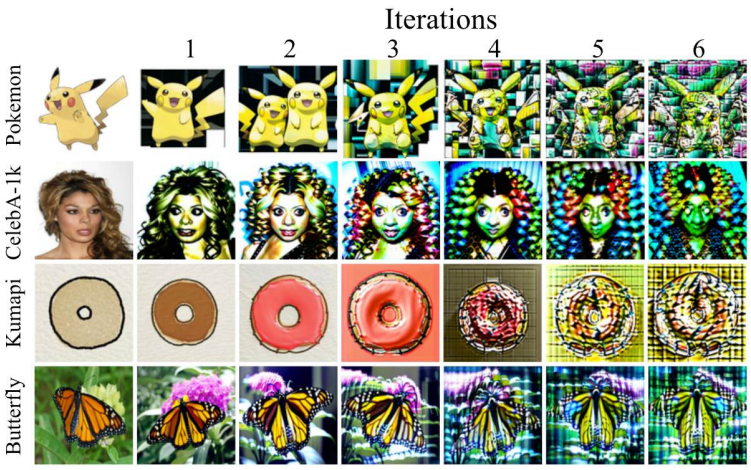


Figure 22: Chain of Diffusion of SDXL on Pokemon dataset. Due to insufficient investigation into optimal hyperparameters for finetuning SDXL, our experiments largely rely on those from Stable Diffusion v1.5.

When Gaussian distribution with mean μ and variance σ^2 is truncated on both sides with r_1 and r_2 ratios, the mean and variance of truncated Gaussian distribution are expressed as:

$$\mu_{trun} = \mu - \frac{\varphi(\beta) - \varphi(\alpha)}{\Phi(\beta) - \Phi(\alpha)}\sigma, \tag{7}$$

$$\sigma^2_{trun} = (1 - \frac{\beta\varphi(\beta) - \alpha\varphi(\alpha)}{\Phi(\beta) - \Phi(\alpha)} - (\frac{\varphi(\beta) - \varphi(\alpha)}{\Phi(\beta) - \Phi(\alpha)})^2)\sigma^2, \tag{8}$$

where φ and Φ are the probability density function (PDF) and cumulative distribution function (CDF) of the standard normal distribution, and $\alpha = \Phi^{-1}(r_1)$ and $\beta = \Phi^{-1}(1 - r_2)$. Accordingly, given $\mu = \mu_t$ and $\sigma^2 = \sigma^2_{P,t}$ with $\mu'_t = \mu_{trun}$ and $\sigma^2_{G,t+1} = \sigma'^2_{P,t} = \sigma^2_{trun}$, we have

$$\Delta\mu_t = h^2_t(\mu'_t - \mu_t) = \frac{\sigma^2_{G,t}}{\sigma^2_{P,t}} c_1\sigma_{P,t} = c_1\frac{\sigma'^2_{P,t-1}}{\sigma^2_{P,t}}\sigma_{P,t} = c_1c_2\frac{\sigma^2_{P,t-1}}{\sigma^2_{P,t}}\sigma_{P,t}, \tag{9}$$

where $c_1 = |\frac{\varphi(\beta)-\varphi(\alpha)}{\Phi(\beta)-\Phi(\alpha)}|$ and $c_2 = 1 - \frac{\beta\varphi(\beta)-\alpha\varphi(\alpha)}{\Phi(\beta)-\Phi(\alpha)} - (\frac{\varphi(\beta)-\varphi(\alpha)}{\Phi(\beta)-\Phi(\alpha)})^2$ when $r_1 > r_2$. On the other hand, the mean phenotypes decreases when $r_1 < r_2$ as:

$$\Delta\mu_t = -c_1c_2\frac{\sigma^2_{P,t-1}}{\sigma^2_{P,t}}\sigma_{P,t}. \tag{10}$$

Furthermore, the phenotype variance converges over time as:

$$\sigma^2_{P,t} = \sigma^2_{G,t} + \sigma^2_E = \sigma'^2_{P,t-1} + \sigma^2_E = c_2\sigma^2_{P,t-1} + \sigma^2_E. \tag{11}$$

$$\sigma^2_{P,t} - \frac{\sigma^2_E}{1 - c_2} = c_2(\sigma^2_{P,t-1} - \frac{\sigma^2_E}{1 - c_2}) = \cdots = c^t_2(\sigma^2_{P,0} - \frac{\sigma^2_E}{1 - c_2}). \tag{12}$$

As a result, the phenotype variance converges to $\frac{\sigma^2_E}{1-c_2}$ for $0 < c_2 < 1$ (the variance of truncated distribution is smaller than the variance of the original distribution), and the mean asymptotically increases (decreases) by $\frac{c_1c_2}{\sqrt{1-c_2}}\sigma_E$ per iteration when $r_1 > r_2$ ($r_2 > r_1$). □

D.2 Simulation setup

Our simulation aims to demonstrate that our experimental results can be modeled using quantitative trait modeling. We show that the radial sum of power spectra of images is one of the phenotypes explained by our theoretical analysis.

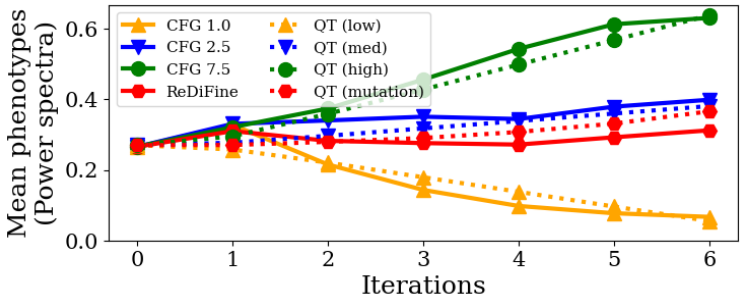


Figure 23: Results comparing the simulation for mutations and power spectra of images generated by ReDiFine (with CFG scale 7.5). Power spectra and simulation are plotted in solid and dotted lines, respectively. Our modifications to heritability and selection process successfully demonstrate changes occur to images by ReDiFine.

D.2.1 Computing the radial sum of power spectra.

The power spectra of images are computed as the square of the magnitude of the 2D Fourier transform. Here, we demonstrate how to compute the radial sum of power spectra in order to use the sum of radial power spectra above a certain threshold. Given a set of images $\{I_i\}$ where $i \in \{1, 2, \cdots, N\}$, the 2D Discrete Fourier Transform (DFT) of an image I_i of size $M \times N$ is computed as:

$$F_i(u,v) = \sum_{x=0}^{M-1} \sum_{y=0}^{N-1} I_i(x,y) e^{-2\pi j (\frac{ux}{M} + \frac{vy}{N})} \tag{13}$$

where $F_i(u,v)$ represents the frequency component at coordinates (u,v). The power spectrum of an image I_i at (u,v) is the square of the magnitude of its Fourier transform $P_i(u,v) = |F_i(u,v)|^2$. We compute the radial sum of the power spectra using a norm of each frequency component (u,v) as $r(u,v) = \sqrt{(\frac{u}{M})^2 + (\frac{v}{N})^2}$. Given the threshold frequency τ, we compute the radial sum of the high-frequency power spectra of an image I_i as

$$S_i = \sum_{u=0}^{M-1} \sum_{v=0}^{N-1} P_i(u,v) \cdot \mathrm{I}(r(u,v) > \tau) \tag{14}$$

where $\mathrm{I}(\cdot)$ is an indicator function. We compute the sum of high-frequency components because low-frequency components tend to be noisy and use the threshold frequency of 0.02. Then, the total sum of power spectra for all images can be written as:

$$S = \sum_{i=0}^{N} S_i = \sum_{i=0}^{N} \sum_{u=0}^{M-1} \sum_{v=0}^{N-1} P_i(u,v) \cdot \mathrm{I}(r(u,v) > \tau). \tag{15}$$

Practically, we shift the Fourier transform maps so that the frequency norm larger than $\frac{1}{\sqrt{2}}$ is considered to be in the opposite direction. Code for detailed implementation comes from the official code of [45].

D.2.2 Simulation parameters matching different CFG scales.

We simulate different selection strategies using truncation ratios r_1 and r_2. To model high, medium, and low CFG scales from our experiments, we apply $(0.025, 0.675)$, $(0.5, 0.09)$, and $(0.95, 0.0002)$ for (r_1, r_2), respectively, which correspond to CFG scales of 7.5, 2.5, and 1.0. For initial values in the simulation, we compute the mean (0.027) and standard deviation (0.056) from the original training set (iteration 0), using them as the initial values for mean and genetic standard deviation for our simulation. We set the environmental standard deviation to 0.25.

D.2.3 ReDiFine and mutations.

ReDiFine combines condition drop finetuning and CFG scheduling, inspired by the mutation mechanism that compensates for distribution shift and maintains genetic distributions in population genetics. We apply two modifications to our theoretical analysis of Section 4—adding mutation variance to heritability and smoothing truncations—to simulate the effects of ReDiFine in the Chain of Diffusion. Specifically, we add the mutation standard deviation σ_M of 0.1 to heritability as:

$$h_t^2 = \frac{\sigma_{G,t}^2}{\sigma_{P,t}^2 + \sigma_M^2} = \frac{\sigma_{G,t}^2}{\sigma_{G,t}^2 + \sigma_E^2 + \sigma_M^2}, \tag{16}$$

representing the randomness added to each iteration due to mutations. This influences the effects of previous iteration to current iteration, which reflect finetuning. Moreover, we apply exponential tails to truncations instead of cut-off thresholds where samples outside the truncation area can be randomly selected with exponential distribution ($e^{-\alpha d(x)}$ where $d(x)$ is a distance to truncation zone and we use $\alpha = 0.1$). This modified selection simulates the effect of CFG scheduling during image generation.

Figure 23 shows the effects of two modifications to our simulation results, and they closely align with the power spectra of images generated by ReDiFine. This demonstrates that the effects of ReDiFine can be understood as interference similar to mutations in population genetics. This suggests further research on model collapse motivated from other fields like biology.

E ReDiFine

Figure 24, 25, 26, and 27 show how robust ReDiFine is to different CFG scales. It successfully mitigates the high-frequency degradations for a wide range of CFG scales.

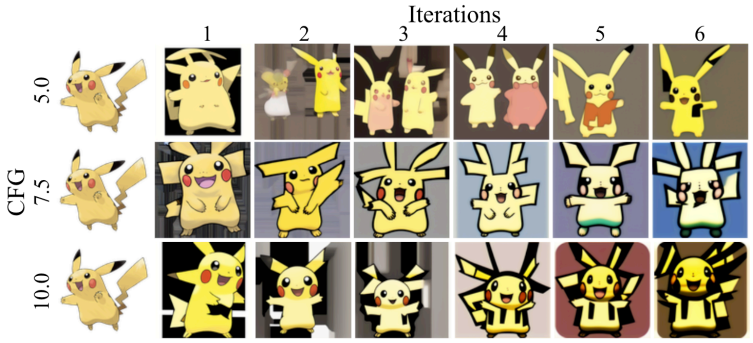


Figure 24: Chain of Diffusion of ReDiFine with different CFG scales on Pokemon dataset. ReDiFine successfully achieves robust image qualities for varying CFG scales.

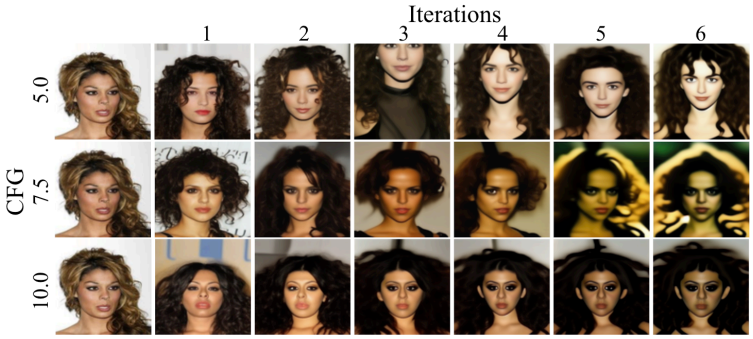


Figure 25: Chain of Diffusion of ReDiFine with different CFG scales on CelebA-1k dataset. ReDiFine successfully achieves robust image qualities for varying CFG scales.

In addition to visual inspections for images generated using ReDiFine, we compare the quantitative results of ReDiFine to baselines with different CFG scales across FID and CLIP score. Furthermore, we compute the average sample-wise feature distance (SFD) between a pair of images corresponding to the text prompt as the fidelity metric applicable for text-to-image generation,

$$\mathrm{SFD}_k = \frac{1}{N} \sum d(f(x_{k,i}), f(x_{0,i})) \tag{17}$$

to evaluate each iteration k. SFD overcomes the problem of FID being sensitive to the number of images to compare. DiNOv2 features are used to compute SFD. The results, shown in Figure 28, demonstrate that ReDiFine achieves performance comparable to the optimal CFG scales (2.5 for Pokemon and Kumapi, 1.5 for CelebA-1k and Butterfly) across different datasets and metrics.

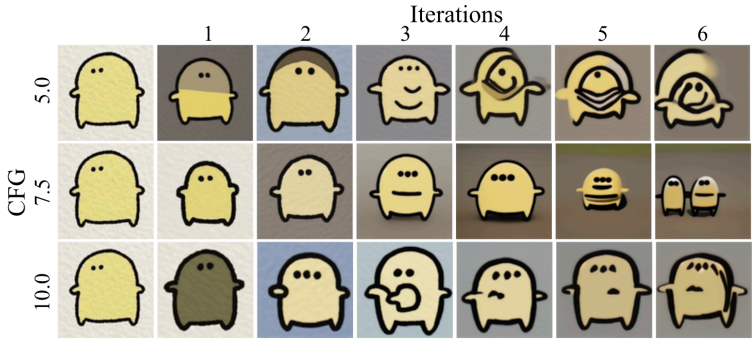


Figure 26: Chain of Diffusion of ReDiFine with different CFG scales on Kumapi dataset. ReDiFine successfully achieves robust image qualities for varying CFG scales.

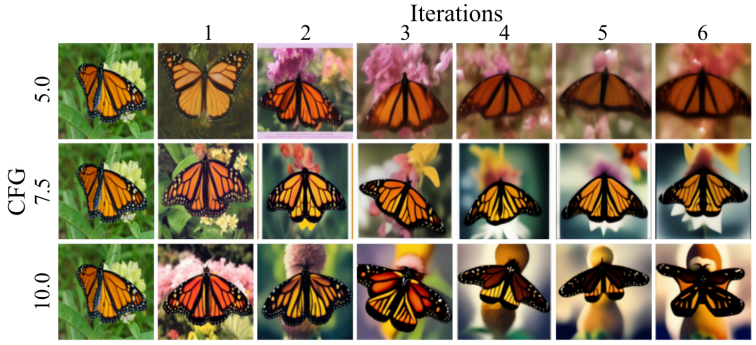


Figure 27: Chain of Diffusion of ReDiFine with different CFG scales on Butterfly dataset. ReDiFine successfully achieves robust image qualities for varying CFG scales.

F Ablation study

This section provides an ablation study to understand how condition drop finetuning and CFG scheduling contribute to the success of ReDiFine.

F.1 Condition drop finetuning

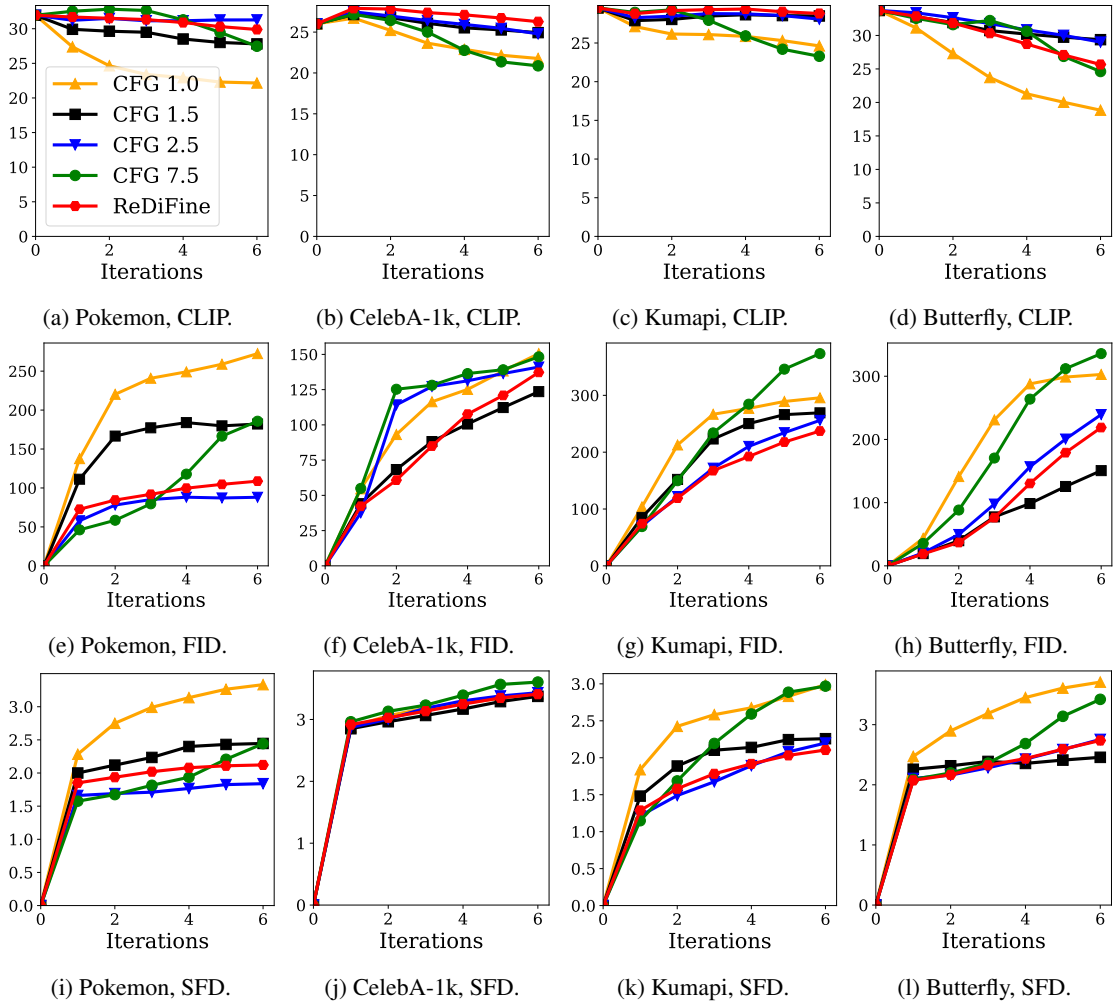
We conducted an ablation study to understand how the probability of dropping text embedding during finetuning affects the image quality in the Chain of Diffusion. We examine 0.1, 0.2, and 0.4 as Stable Diffusion is trained using 0.1 or 0.2. For both Pokemon and CelebA-1k datasets, a probability of 0.2 works the best, as shown in Figure 29 and Figure 30, respectively. Interestingly, condition drop finetuning helps to mitigate the color saturation problem, but its effect decreases with a higher probability. For both of these datasets, condition drop finetuning can mitigate image degradation to some degree, but still, there is a large quality degradation that needs to be improved.

F.2 CFG scheduling

We also evaluated how different CFG scale decreasing strategies impact image degradation in the Chain of Diffusion. We experimented with two different exponential decay rates and compared them with a linear decreasing strategy. Figure 31 demonstrates that CFG scheduling is effective for Pokemon dataset, generating high-quality images comparable to those generated by ReDiFine. However, as shown in Figure 32, it fails to enhance image quality on CelebA-1k dataset. This highlights the necessity of condition drop finetuning for achieving universal improvements in the Chain of Diffusion across various datasets.

G Analysis

In this section, we present a series of analyses of images generated through the Chain of Diffusion. Specifically, we examine the distribution of latent values and the differences between conditional and unconditional scores. Additionally,



(a) Pokemon, CLIP. (b) CelebA-1k, CLIP. (c) Kumapi, CLIP. (d) Butterfly, CLIP.

(e) Pokemon, FID. (f) CelebA-1k, FID. (g) Kumapi, FID. (h) Butterfly, FID.

(i) Pokemon, SFD. (j) CelebA-1k, SFD. (k) Kumapi, SFD. (l) Butterfly, SFD.

Figure 28: Quantitative results of ReDiFine and baselines (different CFG scales).

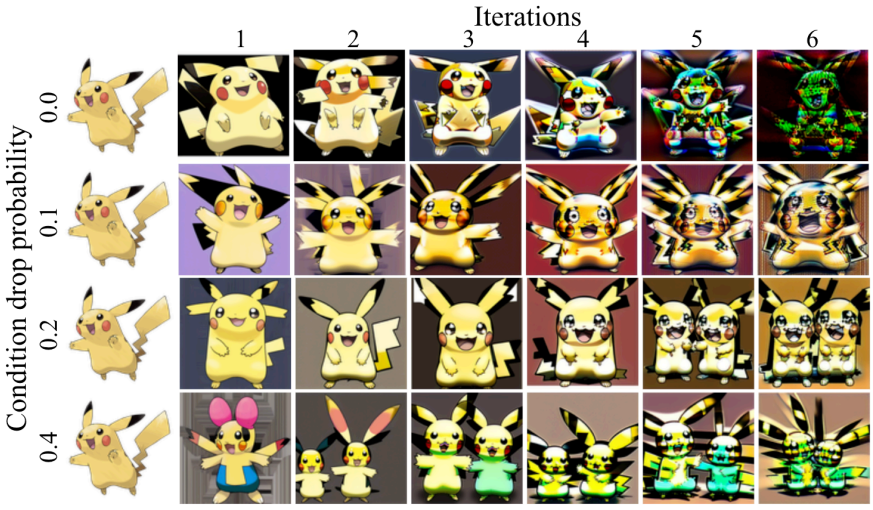


Figure 29: Chain of Diffusion with condition drop finetuning on Pokemon dataset.

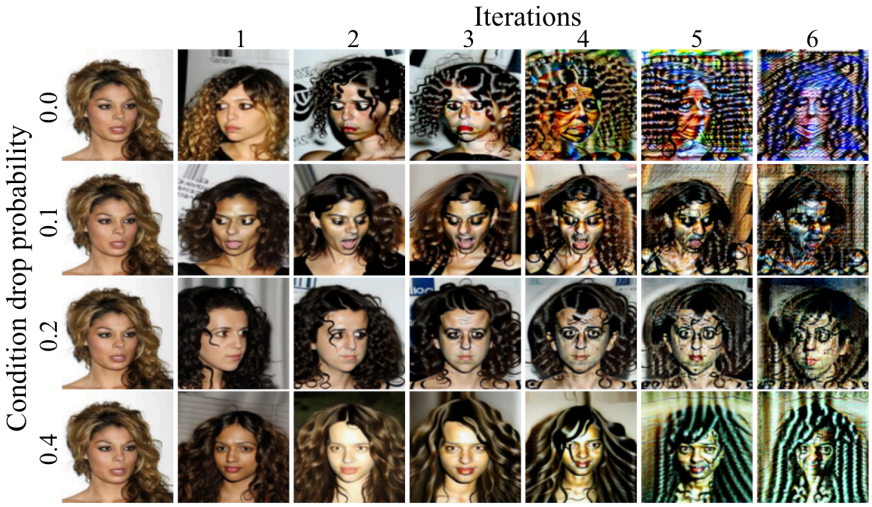


Figure 30: Chain of Diffusion with condition drop finetuning on CelebA-1k dataset.

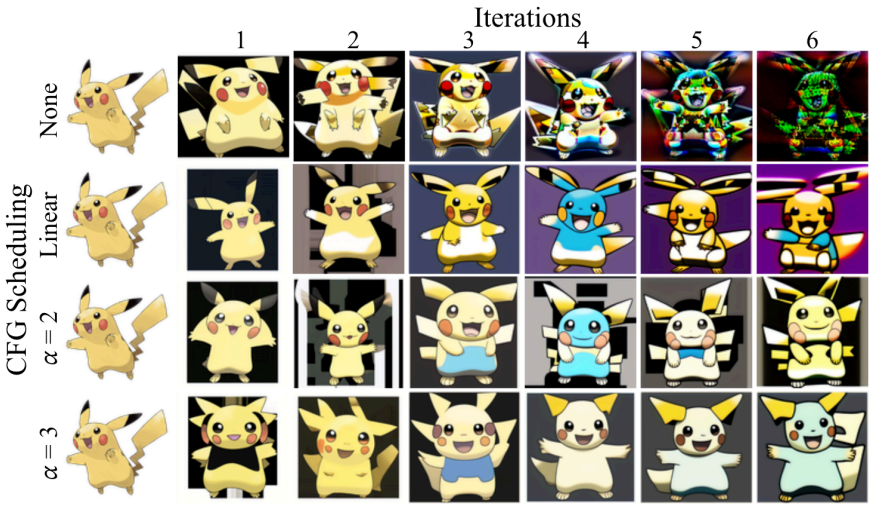


Figure 31: Chain of Diffusion with CFG scheduling on Pokemon dataset.

we analyze the power spectra of the images using 2D Fourier transforms and explore fingerprints through forensic analysis [45, 46].

G.1 Latent analysis

Figure 33(a) illustrates how the distribution of latent values evolves across different iterations. The histograms show the final latent vectors before decoding into pixel space, comparing various CFG scales and ReDiFine. For a CFG of 1.0, the latent distribution rapidly converges into a Gaussian-like shape, with its variance shrinking over iterations. This behavior is consistent with previous work [3, 11, 16], which theoretically predicted that the self-consuming loop progressively trims the tails of the distribution, reducing output diversity until it collapses to a single mode. We hypothesize that this narrowing in the latent space leads to blurrier, more homogeneous outputs in pixel space. Conversely, at a CFG scale of 7.5, the latent distribution develops longer tails and tends toward a more uniform spread across space. A CFG scale of 2.5, which demonstrates the best reusability among the three, better preserves the latent distribution over iterations. ReDiFine further enhances this preservation, maintaining the histogram from the first to the last iteration, thus achieving both high fidelity in the first iteration and better reusability.

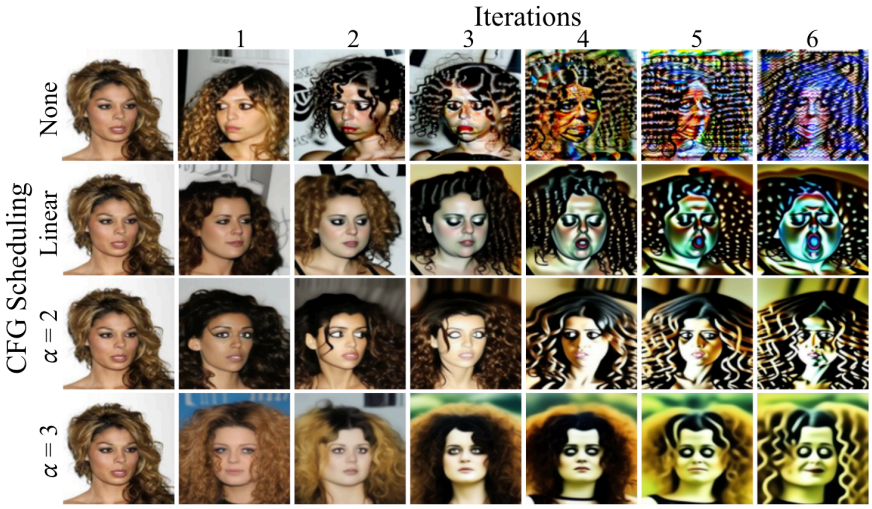
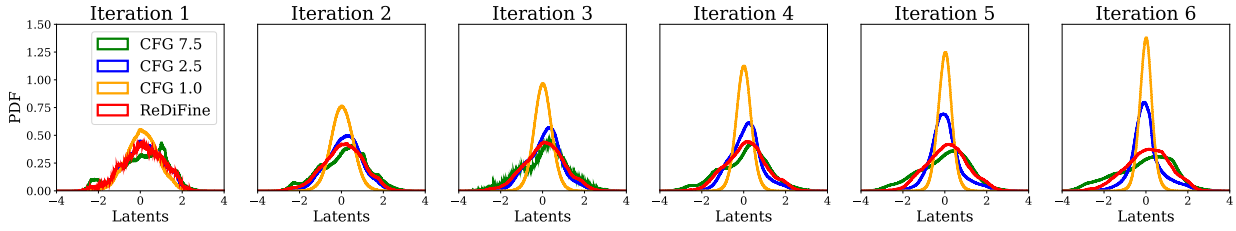
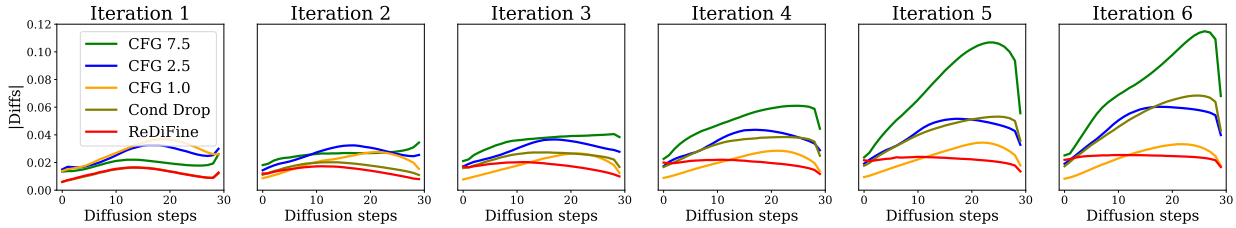


Figure 32: Chain of Diffusion with CFG scheduling on CelebA-1k dataset.



(a) Probability density function (PDF) of values of latent vectors at the last diffusion step.



(b) Norm of differences between conditional and unconditional scores during diffusion steps.

Figure 33: Histogram of latent values and Diffs during diffusion steps for Pokemon dataset. (a) **Latent distribution shrinks over iteration for low CFG and expands with high CFG.** Larger values in latent vectors are more likely to occur with high CFG, gradually increasing the tail of the distribution. (b) **Differences between conditional and unconditional scores increase as the training set is more degraded.** Especially, high differences in the later diffusion steps can be a cause of high-frequency degradation.

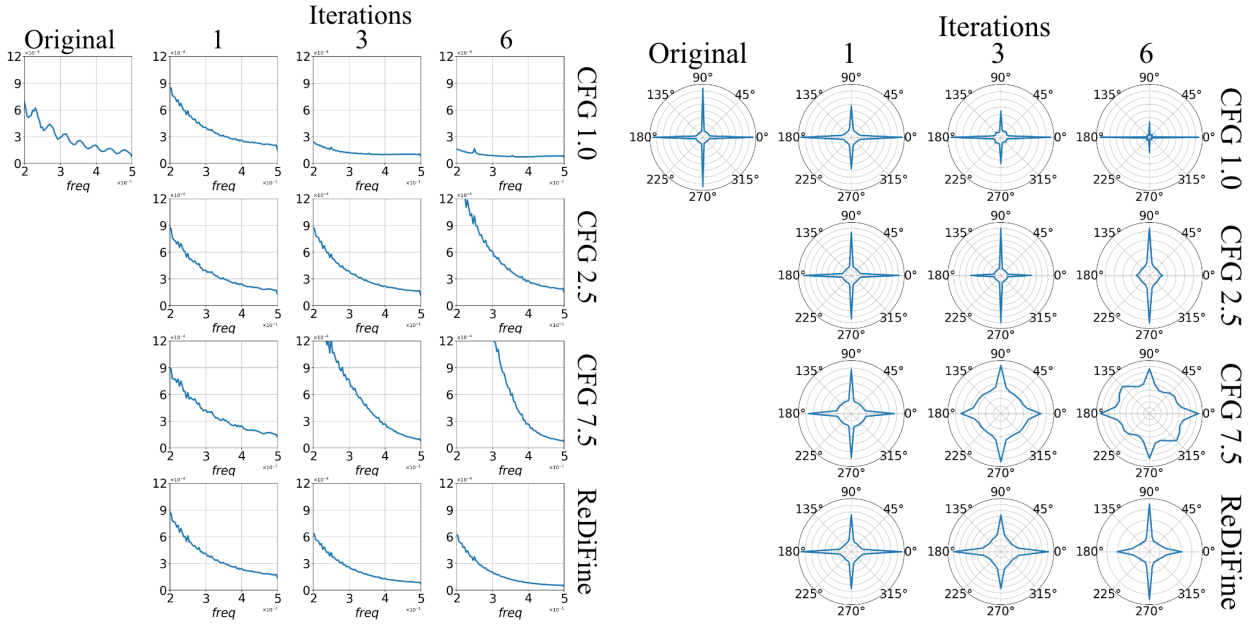
G.2 Differences between conditional and unconditional scores

Next, we plot the evolution of the average norm of Diff (= Cond Score − Uncond Score) across diffusion steps for different iterations in Figure 33(b). In the first iteration, the highest Diff value is observed for CFG 1.0, followed by CFG 2.5 and CFG 7.5. This behavior can be interpreted as the models' adaptive behavior to preserve the values added to the latent vectors, Diff multiplied by CFG scale, at each step. However, this trend shifts in later iterations. The Diff value for CFG 7.5 continues to grow with each iteration, and by iteration 6, we see elevated Diff values throughout the entire diffusion steps, creating a significant gap compared to CFG 2.5 and 1.0. We conjecture that this accumulation of Diff is the responsible for the high-frequency degradation in images generated with CFG 7.5. In contrast, the Diff value for CFG 1.0 remains relatively stable or even decreases across iterations. The deviation of Diff among different iterations is minimized by ReDiFine, which explains its ability to preserve image quality in later iterations. While condition drop finetuning helps reduce the Diff in the earlier iterations, it fails to prevent accumulations in later iterations. This limitation is also evident in the ablation study, where condition drop finetuning alone was insufficient to

prevent model collapse. Notably, ReDiFine produces significantly smaller Diff values compared to the baseline with CFG scale 2.5, comparable to CFG scale 1.0 even when using a high CFG scale 7.5. This underscores the importance of combining condition drop finetuning with CFG scheduling.

G.3 Power spectra of 2D Fourier transforms

Figure 34 demonstrates the radial and angular spectrum power density of both the original and synthetic images. It is evident that ReDiFine closely maintains the radial spectrum power density of the original training set, whereas even a CFG scale 2.5 falls short. Additionally, ReDiFine demonstrates stable angular spectra throughout the Chain of Diffusion, even though they differ from those of the original training set. Pokemon dataset is used for power spectra analysis.



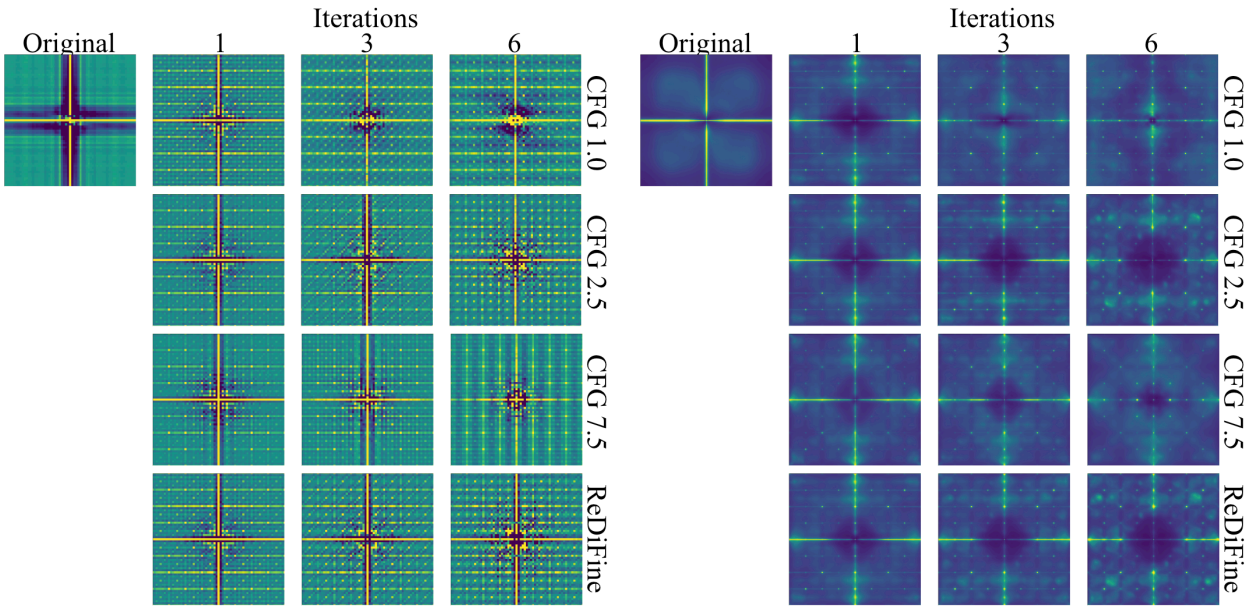
(a) Radial spectrum power density.

(b) Angular spectrum power density.

Figure 34: Power spectrum density of the original training set and synthetic sets for Pokemon dataset. **Images generated by ReDiFine maintain power density distribution during Chain of Diffusion while baselines fail. Even CFG scale 2.5 cannot maintain the distribution for the last iteration.** (a) Radial spectrum power density. ReDiFine shows a density distribution similar to that of the original training set. (b) Angular spectrum power density. Power density of generated images by ReDiFine remains during the iterations while baselines cannot maintain angular distribution.

G.4 Fingerprints for forensic analysis

Several works [45, 46] aim to identify fingerprints of synthetic images. High-quality synthetic images from different generative models have clearly distinct fingerprints, showing the potential to be used for synthetic image detection. We analyze fingerprints of synthetic images for different CFG scales and iterations, and compare them to fingerprints of the original training set. Both autocorrelation and average power spectra show clear differences between the original training set and synthetic images, as shown in Figure 35. Moreover, how the fingerprints of synthetic images evolve throughout the Chain of Diffusion differ for ReDiFine and different CFG scales. Specifically, fingerprints of synthetic images from ReDiFine are similar to those of images from CFG scale 2.5, while other CFG scales (1.0 and 7.5) make fingerprints different from the first iteration as iterations proceed. Horizontal and vertical lines in autocorrelation gradually disappear and central regions in power spectra vary for further iterations. Also, the varying central regions in power spectra imply that low frequency features increase and decrease for CFG scale 1.0 and 7.5, respectively, aligning with visual inspections. Generating images with fingerprints similar to those of the original real images can be an interesting future direction to reduce the degradation in the Chain of Diffusion. Pokemon dataset is used for fingerprint analysis.



(a) Autocorrelation.

(b) Average power spectra.

Figure 35: **The fingerprints of the original training set and synthetic sets show clear differences, and ReDiFine produces fingerprints similar to CFG scale 2.5.** (a) Autocorrelation of image fingerprints. Horizontal and vertical lines gradually disappear for CFG scales 1.0 and 7.5 while they are maintained for CFG scale 2.5 and ReDiFine. (b) Average power spectra of images. Central regions are amplified or diminished for CFG scales 1.0 and 7.5, demonstrating low and high-frequency degradation.